A Dissertation for the Degree of Doctor of Philosophy

Development of Anti-Cancer Therapeutic Strategy Using Synthetic Non-Viral Carriers for Gene and Drug Delivery in Targeted Cancers

February 2017

By

Nomundelger Gankhuyag

Department of Veterinary Medicine

Graduate School of Seoul National University

Development of Anti-Cancer Therapeutic Strategy Using Synthetic Non-Viral Carriers for Gene and Drug Delivery in Targeted Cancers

By Nomundelger Gankhuyag

Supervised by Professor Je-Yeol Cho, D.V.M., Ph.D.

A Dissertation Submitted to the Faculty of the Graduate School of Seoul National University in Partial Fulfillment of the Requirements for the Degree of Doctor of Philosophy in Veterinary Medicine

October 2016

Supervisory Committee Approval of Thesis Submitted by

December 2016

Chairman of Committee: _____

Vice Chairman of Committee: _____

Member of Committee: _____

Member of Committee: _____

Member of Committee: _____

Abstract

Development of Anti-Cancer Therapeutic Strategy Using Synthetic Non-Viral Carriers for Gene and Drug Delivery in Targeted Cancers

(Supervisor: Je-Yeol Cho, D.V.M., Ph.D.)

Nomundelger Gankhuyag

Department of Veterinary Medicine

Graduate School of Seoul National University

Despite significant advances in cancer therapy, cancer continues to be a leading cause of death in the world. One of the major hurdles in cancer therapy is abnormal cancer cell proliferation leading to metastasis.

Traditional cancer therapies are based on the fact that rapidly proliferating cancer cells are more sensitive to anti-cancer drugs, but unfortunately, these anti-cancer drugs show non-specific toxicity to proliferating normal cells too. Therefore, apart from the understanding the molecular basis of cancer, it is now necessary to explore and develop new anti-cancer therapeutic strategy by using non-viral carrier for gene and drug delivery. In first study, lithocholic acid (LCA), a potent anti-cancer drug, is converted to two forms of poly(ethyleneglycol) PEG conjugates, PEG-LCA(PL) and lactobionic acid (LBA) conjugated PEG-LCA (LPL). HepG2 cancer cells and LO2 normal cells were used for *in vitro* experiments. We further confirmed C6-loaded PL and C6-loaded LPL nanoparticles were injected into in H-ras model mice through IV administration.

In another study, we performed the gene therapeutic effect of short hairpin Rab25 RNA (shRab25) on 4-(Methylnitrosamino)-1-(3-pyridyl)-1-butanone (NNK)- induced lung tumorigenesis in female A/J mice. Mice were injected with single dose of NNK by intraperitoneal injection to induce the tumor. Eight weeks later, Glycerol proxylate triacrylate and spermine (GPT-SPE) which is used for non-viral cationic carrier that can deliver gene to lung via aerosol delivery. GPT-SPE/Rab25 using short hairpin RNA complexes delivered into tobacco-induced lung cancer model A/J mice through aerosol-only inhalation twice a week for 8 weeks. Aerosol mediated

gene delivery performs a noninvasive alternative for the targeting genes to lungs. Repeated aerosol delivery of GPT-SPE/Rab25 shRNA complexes greatly suppressed lung tumorigenesis. Those results strongly provide the novel and potential therapeutic outcome for liver and lung cancer treatment.

Key words: anti-cancer drug, apoptosis, hepatocyte-specific, nanoparticles, lithocholic acid, aerosol-delivered shRab25, lung cancer, gene therapy.

Student number: 2012-30770

Contents

List of Figures

Chapter I. Galactosylated-poly(ethyleneglycol)-lithocholic acid selectively kills hepatoma cells, while sparing normal liver cells

and NNK+GPT-SPE/shScr). (C) Total tumor volume ($^{**}p < 0.01$ compared to NNK control and NNK+GPT-SPE/shScr). (D) Histopathological features (magnification, 100×and 200×).

Figure 3. Inhibition of cell proliferation by aerosol delivery of shRab25. (A) Western blot analysis of PCNA. (B) Quantification of PCNA expression. Bands were analyzed by densitometer (n = 3, $^{**}p < 0.01$ compared to NNK control, NNK+GPT-SPE only, and NNK+GPT-SPE/shScr. $^{\#}p < 0.05$ compared to saline control).

(C) PCNA immunohistochemistry analysis (magnification, 400×). (D) PCNA counting (n = 3, $^{**}p < 0.01$compared to NNK control, $^{***}p < 0.001$ compared GPT-SPE only and GPT-SPE/shScr, $^{\#\#\#}p < 0.001$ compared to saline control, $^{\#\#}p < 0.01$ compared to saline control). PCNA, proliferating cell nuclear antigen.

Figure 4. Determination of apoptosis mechanism by aerosol delivery of shRab25. (A, C)

Western blot analysis. Statistical analysis of western blot (B) Rab25 (n = 3, $^{**}p < 0.01$ compared to NNK control). (D) Bcl-2 (n = 3, $^{*}p < 0.05$ compared to NNK control, NNK+GPT-SPE only, NNK+GPT-SPE/shScr, $^{\#}p<0.05$ compared to saline control). (E) Bax (n = 3, $^{\#\#}p<0.01$ compared to saline control). (F) Colorimetric TUNEL assay.

List of Tables

Chapter II. Suppression of tobacco carcinogen-induced lung tumorigenesis by aerosol-delivered GPT-SPE/shRab25 complex in female A/J mice

Table 1. Summary of tumor incidence in NNK treated A/J mice

$^{**}p < 0.01$ compared to NNK group, $^{\#}p < 0.05$ compared to GPT-SPE only, $^{\$\$\$}p < 0.001$ compared to GPT-SPE/shScr. GPT-SPE, glycerol propoxylate triacrylate-spermine; NNK only, mice induced with NNK as a positive control; NNK+GTP-SPE only, mice induced with NNK and treated with GPT-SPE copolymer; NNK+GTP-SPE/shScr, mice induced with NNK and treated with GPTSPE/shScr complex; NNK+GTP-SPE/shRab25, mice induced with NNK and treated with GPT-SPE/shRab25 complex; shRab25, short hairpin Rab25 RNA; STD, standard deviation

List of Abbreviation

Bad	Bcl-2-associated death promoter protein
Bax	Bcl-2-associated X protein
Bcl-2	B-cell lymphoma 2
CCK8	Cell counting kit 8
C6	Coumarin 6
DAB	3,3′-Diaminobenzidinetetrahydrocholoride
DCC	*N,N′*-dicyclohexylcarbodiimide
DLS	Dynamic light scattering
DMEM	Dulbecco's modified Eagle medium
DMSO	Dimethylsulfoxide
FBS	Fetal bovine serum
FTIR	Fourier transform infrared spectroscopy
GPT-SPE	Glycerol propoxylate triacrylate and spermine

H&E	Hematoxylin and Eosin
HRP	Horseradish peroxidase
IHC	Immunohistochemistry
i.p	intraperitoneal
i.v	intravenous
LBA	Lactobionic acid
LCA	Lithocholic acid
NHS	*N*-hydroxysuccinimide
NNK	4-(Methylnitrosamino)-1-(3-pyridyl)-1-butanone
PBS	Phosphate buffered saline
PCNA	Proliferating cell nuclear antigen
PEG	Polyethyleneglycol
PEI	Polyethyleneimine
qPCR	Quantitative PCR
RNAi	RNA interference

ROS	Reactive oxygen species
SDS-PAGE	Sodium dodecyl sulfate-polyacrylamide gel electrophoresis
shRab25	shRNA construct targeting Rab25
shRNA	Short hairpin RNA
TEM	Transmission electron microscopy
TTBS	Tris-buffered saline +Tween 20

General introduction

Hepatocellular carcinoma (HCC) has become one of the serious reason of liver cancer with low 5-year survival worldwide (Li et al., 2016). The liver is important organ in human body, is removing many toxins and chemical waste products from our blood . Therefore, lung cancer is the leading cause of c ancer deaths worldwide, especially due to tobacco smoking that causes nearly 6 million deaths per year. Despite significant advances in cancer therapy, cancer continues to be a leading cause of death in the world. Multiple therapies have been proposed to target cancers still needed urgent therapy.

I tried to develop anti-cancer therapeutic strategy using polymeric vector based drug and gene delivery, those have been responsible for targeted cancers. Polycationic vector polymers have been attracted to increase application for gene and drug delivery last two decades (Cordeiro et al.). To make a nanoparticle formulation, drugs can be either encapsulated into a polymeric vehicle or chemically attached to PEG in a process called pegylation. The latter process also improves the pharmacokinetic and pharmacodynamic properties of drugs by increasing water solubility, reducing renal clearance and limiting toxicity (Harris and Chess, 2003).

Lithocholic acid is a naturally occurring secondary bile acid that is formed in the gut during bacterial degradation of the primary bile acids and metabolized in liver (Nicholson et al., 2012). Bile acids are steroidal amphipathic molecules that facilitate excretion, absorption, and transport of fats and sterols in the intestine and liver (Patil et al., 2013). Although some bile acid derivatives have been identified to exhibit potent cytotoxic properties, (Kozoni et al., 2000) recent researches suggest that LCA not only kills neuroblastoma cells selectively, but also displays anti-tumor effect in several types of cultured cancer cells at physiologically relevant concentrations (Goldberg et al., 2011). Due to versatile properties of LCA, i aimed to design a nanoparticle formulation of LCA as PEG conjugate and test the efficacy of the formulation for enhanced antitumor effect.

Furthermore, tobacco contains a variety of carcinogens, of whi ch NNK has been identified as the most potent lung carcinogen (Schu ller et al., 2003). It is noted that a single IP injection of NNK at a dose of 2 mg is enough to induce an average of 10–12 lung adenom as per A/J mouse (Hecht et al., 1989). Hence, A/J mouse is a suitabl e model to study the molecular mechanisms of NNK to induce the de velopment and progression of lung tumors. Based on these animal mo dels, although many antitumor agents have been identified to suppress the NNK-induced lung carcinogenesis to some extent, it is still neces

sary to develop advanced methods to treat the lung cancer at genetic level. It has been reported that chromosome instability, genetic mutatio n, and activation of oncogenes are occurred in NNK-induced lung tum ors due to disruption of the expression of several enzymes of various cellular signal pathways (Zheng and Takano, 2011).

Many scientists have therefore largely focused on RNA interfe rence (RNAi)-based knock down for cancer therapy. Usually, two kind of RNAi-based therapeutics are well-known: a vector-based short hairpin RNA (shRNA) based on a vector or a chemically synthesized double-stranded small interfering RNA (siRNA) (Rao et al., 2009). Aerosol-mediated gene delivery performs a noninvasive alternative for the targeting of genes to the lungs (Merlin JL, 2001).

Rab25 signaling pathway plays a role in the regulation of cell proliferation and apoptosis in cancer cells indicating that the Rab25 gene plays an important role in tumor occurrence and development (Agola et al., 2011). Rab25 belongs to the Rab-related small guanosine triphosphatase (GTPases) proteins; these proteins are considered key regulators of intracellular membrane trafficking involved in various diseases, including cancer (Subramani and Alahari, 2010; Tanos and Rodriguez-Boulan, 2008).

Several Rab GTPases, including Rab25, have been examined for being potential drivers in carcinogenesis (Luen Tang, 2010).

Glycerol proxylate triacrylate and spermine (GPT-SPE) which is used for non-viral cationic carrier that can deliver gene to lung via aerosol delivery. GPT-SPE has been known to good delivery efficiency of shRNA and have less toxicity than PEI-25K(Jiang et al., 2011). Cationic polymers are easy to be improved their molecular weight, surface charge, and other characterizations (Merdan et al., 2002). Gene therapy as a promising treatment strategy for cancer, aerosol delivery of therapeutic genes seems the most convenient way for lung cancer gene therapy because it is simple, non-invasive and direct method that makes instant access to lungs without any effect to other organs due to the anatomical structure and location of the lungs inside the body (Gautam et al., 2003).

Chapter I

Galactosylated-Poly(Ethyleneglycol)-Lithocholic Acid Selectively Kills Hepatoma Cells, While Sparing Normal Liver Cells

(Published in 2015, Macromolecular Bioscience)

Abstract

Delivering drugs selectively to cancer cells but not to nearby normal cells is a major obstacle in drug therapy. Recent reports suggest that lithocholic acid (LCA) is a potent anti-cancer drug that selectively kills cancer cells, sparing normal cells. Although LCA holds great promise for killing cancer cells, it is usually inappropriate for in vivo use because of its low solubility, short shelf life, short circulating half-life, and rapid renal clearance from the body. Conversely, the afore-mentioned defects can be overcome through a process called PEGylation. In this study, LCA was converted to two forms of PEG conjugates, viz., PEG-LCA and Galactose-PEG-LCA. The latter form contains a galactose ligand to target the hepatocytes. Both forms are self-assembled to form nanoparticle formulation, and they have high potency to kill HepG2 cancer cells, sparing normal LO2 cells, similar to the function of LCA as reported before. Besides, Galactose-PEG-LCA had high specificity to HepG2 cells in killing the cells. Western blot results confirmed that the cell death is occurred through apoptosis induced by LCA nanoparticles. Further loading of anti-cancer drugs inside the core of LCA nanoparticles as drug delivery vehicles will be of great importance to evaluate the potential of this system.

Introduction

Despite significant advances in cancer therapy, cancer continues to be a leading cause of death in the world (Jemal et al., 2008). One of the major hurdles in cancer therapy is abnormal cancer cell proliferation leading to metastasis (Chaffer and Weinberg, 2011) Traditional cancer therapies are based on the fact that rapidly proliferating cancer cells are more sensitive to anti-cancer drugs, but unfortunately, these anti-cancer drugs show non-specific toxicity to proliferating normal cells too (Pasut and Veronese, 2009). Therefore, apart from the understanding the molecular basis of cancer, it is now necessary to explore and develop new anti-cancer drugs which are much more selective to cancer cells.

Recently, lithocholic acid (LCA), a bile acid, has been reported to kill human neuroblastoma cells, while sparing normal human primary neurons due to the selective initiation of an extrinsic apoptotic programme of cell death in neuroblastoma cells (Goldberg et al., 2011).

It is now documented that the LCA inhibits the proliferation of prostate cancer cells without killing immortalized normal prostate epithelial cells, where the extrinsic pathway of apoptosis and cell death induced by LCA is partially dependent on the activation of caspase-8 and -3 (Goldberg et al., 2013).

Although LCA holds great promise for killing cancer cells, it is usually

inappropriate for in vivo use because of its low solubility, short circulating half-life, and rapid renal clearance from the body. Conversely, the afore-mentioned defects can be overcome by conjugation of poly(ethylene glycol) (PEG) with drugs through a process called PEGylation that has been identified as a promising strategy in drug delivery system to improve solubility and biocompatibility of the drugs and to facilitate the particle diffusion in biological environments (Cu and Saltzman, 2009; Pendri A, 1996; Vllasaliu et al., 2014)

Moreover, receptor-mediated cellular uptake of the drugs has received much attention in the field of drug delivery systems, (Leamon and Low, 2001; Qian et al., 2002; Sudimack and Lee, 2000) as drugs can be targeted to the specific cells or tissue through the specific interaction of ligands with receptors of the cells (Wagner E. Curiel D, 1994) Accordingly, galactose is one of the most used ligands for targeting liver parenchymal cells because hepatocytes have large number of cell surface receptors called asialoglycoproteins that have high-affinity with galactose moiety (Wu and Wu, 1998)

The present study aims to develop a potent anticancer drug, lactobionic acid (LBA)-PEG-LCA (LPL), for targeted delivery that selectively kills hepatoma cells sparing normal liver cells.

Materials and methods

Chemicals and reagents

Lithocholic acid (LCA), lactobionic acid (LBA), *N,N'*-dicyclohexylcarbodiimide (DCC), *N*-hydroxysuccinimide (NHS), dimethylsulfoxide (DMSO), Coumarin 6 (C6) were purchased from Sigma-Aldrich (USA). Diamino polyethyleneglycol 6000 Da (PEG) was purchased from SunBio (Korea). All reagents were of analytical grade and used without further purification.

Anti-PARP and anti-Caspase-3, anti-Cleaved Caspase-3 antibodies were from Cell Signaling (Beverly, MA, USA). The other indicated anti-β-Actin, anti-Bad antibodies were from Santa Cruz Biotechnology (Santa Cruz, CA, USA).

Synthesis of LPL

LPL was synthesized in two-step reactions (Scheme 1). First, LBA (2 mM) was activated in DMSO (10 ml) with DCC (4 mM) in the presence of NHS (4 mM) at room temperature for 18 h. The activated LBA was then reacted with PEG (20 mM) at room temperature for 4 h. The reaction product was first dialyzed in DMSO using a dialysis membrane (Spectra/Por MWCO: 1,000) for 24 h to remove the unreacted LBA, and finally dialyzed against

water at 4 °C overnight. The first product, LBA-PEG (LP), was freeze dried. To conjugate LCA with LP, LCA (50 mM) was activated in DMSO (10 ml) with DCC (100 mM) in the presence of NHS (100 mM) at room temperature for 18 h. The activated LCA was reacted with LP (10 mM) at room temperature for 4 h. The reaction product, LPL, was first dialyzed in DMSO using a dialysis membrane (MWCO: 1,000) for 24 h to remove unreacted LCA, and finally dialyzed against water at 4 °C overnight. LPL nanoparticles thus formed during dialysis step was collected, and washed with water to remove unreacted water soluble PEG portion. LPL was further freeze dried and stored at -80°C until use. Similarly, C6-loaded PL or LPL nanoparticles were prepared by dialysis method. C6 (0.4 mg) was mixed with PL or LPL (20 mg) in DMSO (5 ml). The mixture was dialyzed in water using Spectra/Por membrane (MWCO: 1,000) at 4 °C overnight. Due to hydrophobic nature of LCA, C6-loaded PL or LPL nanoparticles are formed during dialysis due to the transition from DMSO to hydrophilic medium water. The nanoparticles were freeze dried and stored at -80°C until use.

NMR and FTIR

Each step of the synthesis of LPL and PL was analyzed by ^{1}H NMR spectroscopy (Avance600, Bruker, Germany). Conjugation of LBA or LCA

in LPL and PL was also confirmed by Fourier transform infrared spectrometer (FTIR; Nicolet 6700, Thermo Fisher Scientific Inc., Waltham, MA, USA). The compositions of conjugated molecules in the polymer were determined by ^{1}H NMR as suggested in polymer analysis by NMR (Sigma-Aldrich, Material Matters 2006, 1.1, 3). The mole% of conjugated molecules in the polymer was calculated by the given equation, (Izunobi J. U. , 2011)

$$Z(\%) = \frac{\frac{a_x}{m_x}}{\frac{a_x}{m_x}+\frac{a_y}{m_y}} \times 100\%$$

where a_x is the area of the ^{1}H NMR peak of Z molecule; m_x is the number of protons of Z molecule; a_y is the area of the ^{1}H NMR peak of adjacent molecule in the polymer; and m_y is the number of protons of adjacent molecule.

Physicochemical characterization of LPL nanoparticles

The size of nanoparticles was measured by dynamic light scattering spectrophotometer (DLS 8000, Otsuka Electronics, Osaka, Japan) with 90° scattering angles. The morphology of LPL nanoparticles was observed by energy-filtering transmission electron microscope (EF-TEM) (LIBRA 120, Carl Zeiss, Germany). The nanoparticles in suspension were adsorbed to carbon-coated ionized Formvar grids, negatively stained with 2% uranyl

acetate, and observed with EF-TEM.

Cytotoxicity assay

Normal liver cell line (LO2) and human liver carcinoma cell line (HepG2) were maintained in DMEM medium and RPMI-1640 medium (HyClone, Thermo Scientific, USA), respectively, supplemented with heat-inactivated fetal bovine serum (HyClone, Thermo Scientific, USA) and penicillin/streptomycin (GibcoBRL, Grand Island, USA). All cells were cultured under standard incubation condition at 37°C with 5% CO_2. Cytotoxicity of nanoparticles in LO2 and HepG2 cells was determined by cell proliferation assay using cell counting kit-8 (CCK8) (Dojindo Laboratories, Japan). Briefly, cells were seeded in 96-well plates at an initial density of 4×10^3 cells/well for LO2 and 4×10^3 cells/well for HepG2 in 0.1 ml of growth medium and pre-incubated 24 h prior to addition of filtered substrate. Growth media was replaced by 0.1 ml fresh serum free media containing 50 uM and 100 uM of nanoparticles. After additional incubation for 24 h, 10 ul of CCK8 solution was added to each well of the plate and incubated for 3 h. The absorbance was measured at 450 nm using an ELISA plate reader (plate reader Model 680, BIORAD).

Western blot analysis

Cells were cultured under standard incubation condition at 37°C with 5% CO_2. The samples at the concentration of 50 μM were treated to the cells for 24 h. The mechanism of apoptosis induced by the given samples was determined by observing a number of proteins involved in apoptosis. By measuring and quantifying the protein concentration of cell lysates using a Pierce®BCA Protein Assay kit (Thermo scientific, Rockford, IL 61101 USA), equal amounts (25 μg) of protein were loaded into 10-15% sodium dodecyl sulfate-polyacrylamide gel electrophoresis (SDS-PAGE) gel and transferred to nitrocellulose membranes. Membranes were blocked with TTBS containing 5% skim milk for 1 h at room temperature and immunoblotting was performed by incubation overnight at 4°C with the corresponding primary antibodies in 5% skim milk and then with secondary antibodies conjugated to horseradish peroxide for 4 h at room temperature. After washing, bands-of-interest were visualized using a model EZ-capture MG luminescent image analyzer (ATTO, Tokyo, Japan).

Apoptosis detection by Annexin V-FITC analysis

In addition to western blot, Ezway™ Annexin V-FITC apoptosis detection kit (Komabiotech, Korea) was used to identify the apoptosis induced by the LPL nanoparticles according to the manufacturer's instructions. Cells,

seeded at a density of $2x10^5$ cells in culture flask, were incubated at standard condition for 48 h. The samples (50 μM) were treated to the cells for 24 h. Cells were trypsinized and collected in microtubes by centrifugation at 1000 x g for 5 min. The cells were washed twice with cold phosphate buffer saline (PBS). The cells were further washed with cold binding buffer. The cells were incubated with Annexin V-FITC for 15 min in dark. The cells were washed with binding buffer. Finally, the cells were stained with propidium iodide (PI) and analyzed by flow cytometry immediately.

Ligand specificity of LPL in vivo

The specificity of galactose ligand in the LPL with hepatocytes in vivo was examined using 13 weeks old H-ras mice obtained from the Human Cancer Consortium National Cancer Institute (Frederick, MD). The mice were divided into three groups (four mice/group). The control group was non-treated, and the other two groups were injected to intravenous (IV) vein with C6-loaded PL and LPL nanoparticles respectively. The concentration of C6 was 5 μg per mice. Animals were kept in the laboratory animal facility with temperature and relative humidity maintained at 23°C ± 2°C and 50% ± 10%, respectively, and with a 12 hour light/dark cycle. The mice were sacrificed after 2 h of IV injection, and the organs were collected, fixed in 4% paraformaldehyde, and preserved in 30% sucrose for 3 h at 4°C. Tissues

were embedded and were sectioned with a microtome. The sections of the organs were visualized under fluorescence microscope (Olympus BX51).

Statistical analyses

Statistical analyses were performed with a **student's *t* test** (Graphpad Software, San Diego, CA, USA). $^{*}P < 0.05$ was considered more significant than the corresponding control values.

Results and Discussion

Preparation and characterization of LPL and PL

Bile acids are steroidal amphipathic molecules that facilitate excretion, absorption, and transport of fats and sterols in the intestine and liver (Patil et al., 2013). Although some bile acid derivatives have been identified to exhibit potent cytotoxic properties, (Kozoni et al., 2000) recent researches suggest that LCA not only kills neuroblastoma cells selectively, but also displays anti-tumor effect in several types of cultured cancer cells at physiologically relevant concentrations (Goldberg et al., 2011). Due to versatile properties of LCA, we aimed to design a nanoparticle formulation of LCA as PEG conjugate and test the efficacy of the formulation for enhanced antitumor effect.

Therefore, pegylation of LCA was performed as described in materials and

methods. Firstly, LBA that harbors galactose moiety was activated using DCC/NHS reagents and conjugated with diamino PEG through amide linkage between carboxylic group of LBA and amino group of PEG. Unreacted LBA was removed through dialysis against water. The content of LBA in LP as estimated by ^{1}HNMR was about 10 mol-%. Secondly, LCA was similarly reacted with LP using DCC/NHS through amide linkage between carboxylic group of LCA and amino group of LP (Scheme 1). Unreacted LCA and PEG were removed by dialyzing in DMSO and then washing in water, respectively. The content of LCA in LPL as estimated by ^{1}H NMR was about 63 mol-%. The ^{1}H NMR spectra of PEG, LCA, LBA and LPL are shown in Fig. 1, while ^{1}H NMR spectra of LP and PL in Supplementary Fig. 1.

These results indicate that LBA and LCA were reacted with the two ends of diamino PEG through amide linkages. We further confirmed the amide bonds of LPL by Fourier transform infrared spectroscopy (FTIR) (Fig. 2). The results also indicated the successful synthesis of LPL and PL. Furthermore, we expected that LPL would self-assemble to form polymeric nanoparticles because of amphipathic property of LPL. Indeed, the spherical nanoparticles with particle size of 300-400 nm was observed by TEM as shown in Fig. 3. The mean hydrodynamic diameter of PL and LPL nanoparticles as measured by DLS was 370 nm and 380 nm, respectively

(Fig. 3).

Stability of LPL and PL nanoparticles

The release of active drug from polymer-drug conjugate (prodrug) is important to be used as drug delivery in cancer (Duncan, 2006). However, our aim was to develop PEG-LCA as a permanent polymer-drug conjugate through amide bond. The amide bond is often the bond of choice when linking the polymer to the drug to make permanent polymer drug conjugates because amide bonds are very stable to aqueous hydrolysis at physiological pH, and to enzymatic hydrolysis (D'Souza and Topp, 2004). Therefore, we tested the stability of PL and LPL nanoparticles at physiological condition by incubating the nanoparticles in water at 37°C for 3 days. We did not observe any change in the morphology of the nanoparticles by TEM analysis (Supplementary Fig. 2). The results demonstrated that the nanoformulations of PL and LPL were highly stable. Therefore, we concluded PL and LPL as permanent drugs with no release of LCA from them.

Toxicity of LPL and PL nanoparticles

We tested the toxicity of PL and LPL in LO2 and HepG2 to compare anti-tumor effect between normal and cancer cells. Fig. 4 shows the cell viability of LO2 and HepG2 treated with LCA, PL and LPL at two different

concentrations and incubation periods. The cell viability of LO2 cells at 50 μM concentration of LCA and PL was almost 100% whereas cell viability was about 75% with LPL treatment. On the other hand, the cell viability of HepG2 cells treated with LCA, PL and LPL at 50 μM concentration was 60%, 65% and 20%, respectively.

The results indicated that PL at a concentration of 50 μM is not cytotoxic to normal cells whereas PL killed HepG2 cells, indicating that PL selectively killed cancer cells, while sparing normal cells. Similar effect was observed in our experiment when treated with LCA, as reported before (Goldberg et al., 2011).

Significantly, the efficiency of LPL at 50 μM concentration is 3-fold higher than LCA in killing the cancer cells. Above all, the anti-tumor effect of LPL in HepG2 cells was stronger than that of PL due to the specific interaction between galactose ligands in the LPL and asialoglycoprotein receptors in the HepG2 cells. Treatment of LCA and PL at a concentration of 100 μM in normal cells showed only slight cytotoxicity, whereas the cell viability of HepG2 cells was ≤10%. These results provoked that the nanoparticle formulation of LPL has comparable efficacy with LCA small molecules. It seemed that the mechanism of drug action of LCA is similar with LPL nanoparticles. On the other hand, the cell viability of LO2 cells was ~50% after the treatment of LPL at a concentration of 100 μM, while the cell

viability of HepG2 cells was less than 5%. These results also indicated the efficacy of the nanoparticle formulation of LPL is higher in cancer cells than normal cells.

Ligand specificity of LPL with liver cells in vivo

To evaluate the ligand specificity of LPL in mouse liver cells in vivo, C6-loaded PL and C6-loaded LPL nanoparticles were injected into individual mouse through IV administration. Fig. 5 shows fluorescence images of several organs of mouse after injection of C6-loaded nanoparticles. It was observed that the distribution of LPL nanoparticles in the liver was higher than the distribution of PL. The result clearly depicted the ligand specificity of LPL with the mouse liver in vivo. On the other hand, we did not find any differences between LPL and PL distribution in lung and kidney, probably due to non-specific distribution of both nanoparticles in those organs.

Mechanism of apoptosis induced by LPL nanoparticles

To understand the cellular signaling processes leading to apoptosis induced by LCA nanoparticles, western blot was performed to trace the related enzymes in the signaling processes. During the early phases of apoptosis, caspase-3 is activated by proteolytic cleavage (Thornberry and Lazebnik, 1998). Caspase-3, in turn, cleaves poly (ADP-ribose) polymerase-1 (PARP) into 89-kDa fragments, thereby inactivating it (Krishnakumar and Kraus,

2010). PARP is a 116 kDa enzyme involved in DNA repair and maintenance of genomic integrity (Virág and Szabó, 2002). Therefore, detection of cleaved caspase-3 and/or PARP by western blot is routinely used for the study of apoptosis. Fig. 6 shows the detection of PARP and caspase 3 in LO2 and HepG2 cells after treatment of LCA and LPL nanoparticles as described in materials and methods.

Western blot studies showed that the expression levels of proteins related to apoptosis vary in normal and cancer cells. In contrast to LO2 cells, the blot showed the down-regulation of PARP protein levels and up-regulation of caspase 3 in HepG2 cells. Similarly, the level of Bad protein (pro-apoptotic member of the Bcl-2 family)(Kitada et al., 1998) and even actin protein expressed higher in LO2 cells in compare to HepG2 cells. While the level of cleaved PARP after treatment with LCA, LP and LPL was similar in LO2 cells, the cleaved PARP was distinctly visible in the blot only with the treatment of LPL in HepG2 cells. The cleaved PARP was not clearly visible after the treatment of LCA in HepG2 cells, probably due to very low expression of PARP. However, the expression levels of Bad with the treatment of LPL and LCA were higher in HepG2 cells compared to control. Similarly, in compare to LO2, the expression levels of cleaved caspase-3 in HepG2 cells with the treatment of LCA and LPL were higher.

Although the results elucidated the occurrence of apoptosis with the treatment of nanoformulation of LCA in cancer cells, it seemed that a distinct mechanism of apoptosis occurs in cancer cells in contrast to normal cells. The notion is further supported by a previous report that stated doxorubicin induces apoptosis in normal and tumor cells via distinctly different mechanisms (Wang et al., 2004). The mechanism of LCA-induced apoptosis has been recently explored in several studies. The mechanism of CD95 death receptor activation by bile acids has been studied in hepatocytes and is thought to proceed through the generation of oxidative stress by these steroids (Sokol et al., 2006). Similarly, LCA is able to induce immediate oxidative stress with subsequent generation of reactive oxygen species (ROS) in colon adenocarcinoma cells (Katona et al., 2009).

The study further suggested that LCA-induced apoptosis is proceeded through a mitochondrial/caspase-9-dependent pathway initiated by caspase-8 (Katona et al., 2009).

Most recent study suggested that LCA can directly induce syncytiotrophoblastic apoptosis in vitro, possibly via the TNF-α pathway, with caspase-3 activation (Du et al., 2014).

In this study, with the treatment of LPL, the catalytic activity of PARP and caspase-3 in HepG2 was higher than in LO2, indicating that the mode of

anti-tumor effect of LPL is similar with the apoptosis induced by LCA via a caspase-3-dependent mechanism.

We further determined the apoptosis induction by LPL nanoparticles using Annexin V-FITC staining. As shown in Fig. 7, treatment with PL and LPL induces 1.4 and 3.1-fold increases in apoptotic cells at 50 μM concentrations compared to LCA. It was clearly seen in the figure that the cells underwent early apoptosis and late apoptosis which was comparatively higher when the cells were treated with LPL nanoparticles than LCA. Therefore, Annexin-FITC study also revealed that the nanoformulation of LCA nanoparticles induced high apoptosis resulting high cell death.

Scheme 1

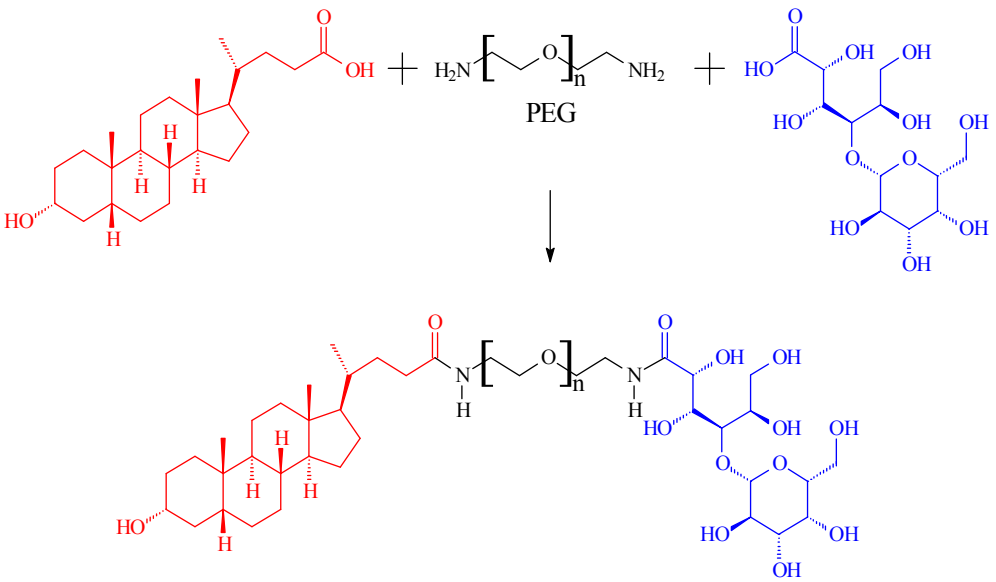

Figure 1

A

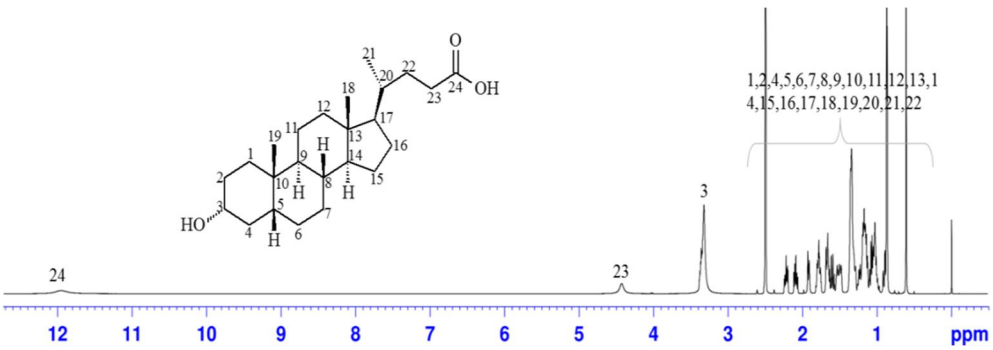
1,2,4,5,6,7,8,9,10,11,12,13,1
4,15,16,17,18,19,20,21,22
24
23
3
12 11 10 9 8 7 6 5 4 3 2 1 ppm

B

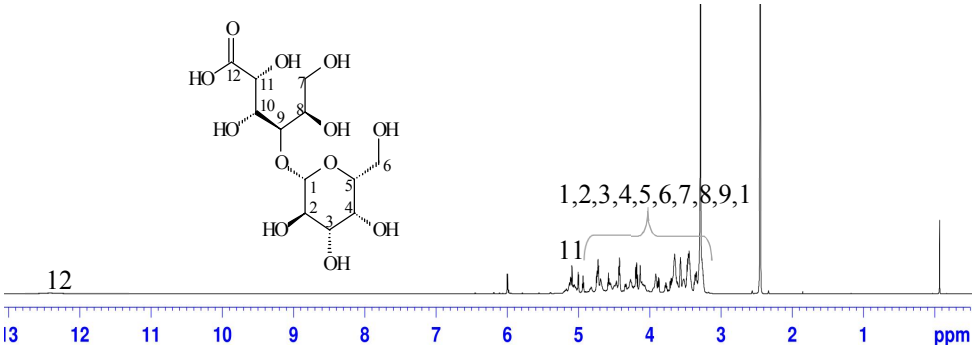
1,2,3,4,5,6,7,8,9,1
11
12
13 12 11 10 9 8 7 6 5 4 3 2 1 ppm

C

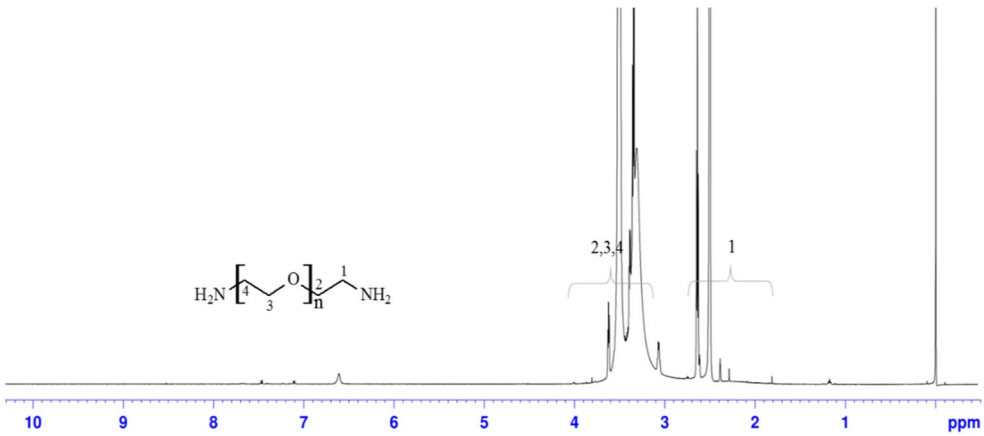

D

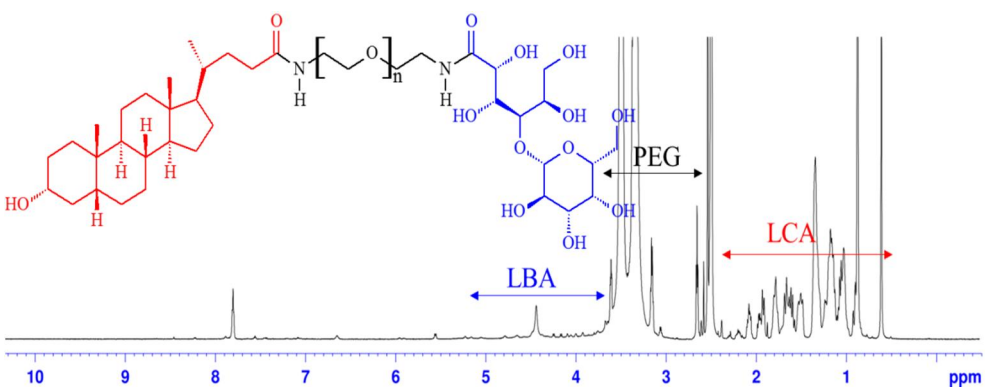

Figure 1. ^{1}H NMR spectra of LCA (A), LBA (B), PEG (C) and LPL (D).

Figure 2

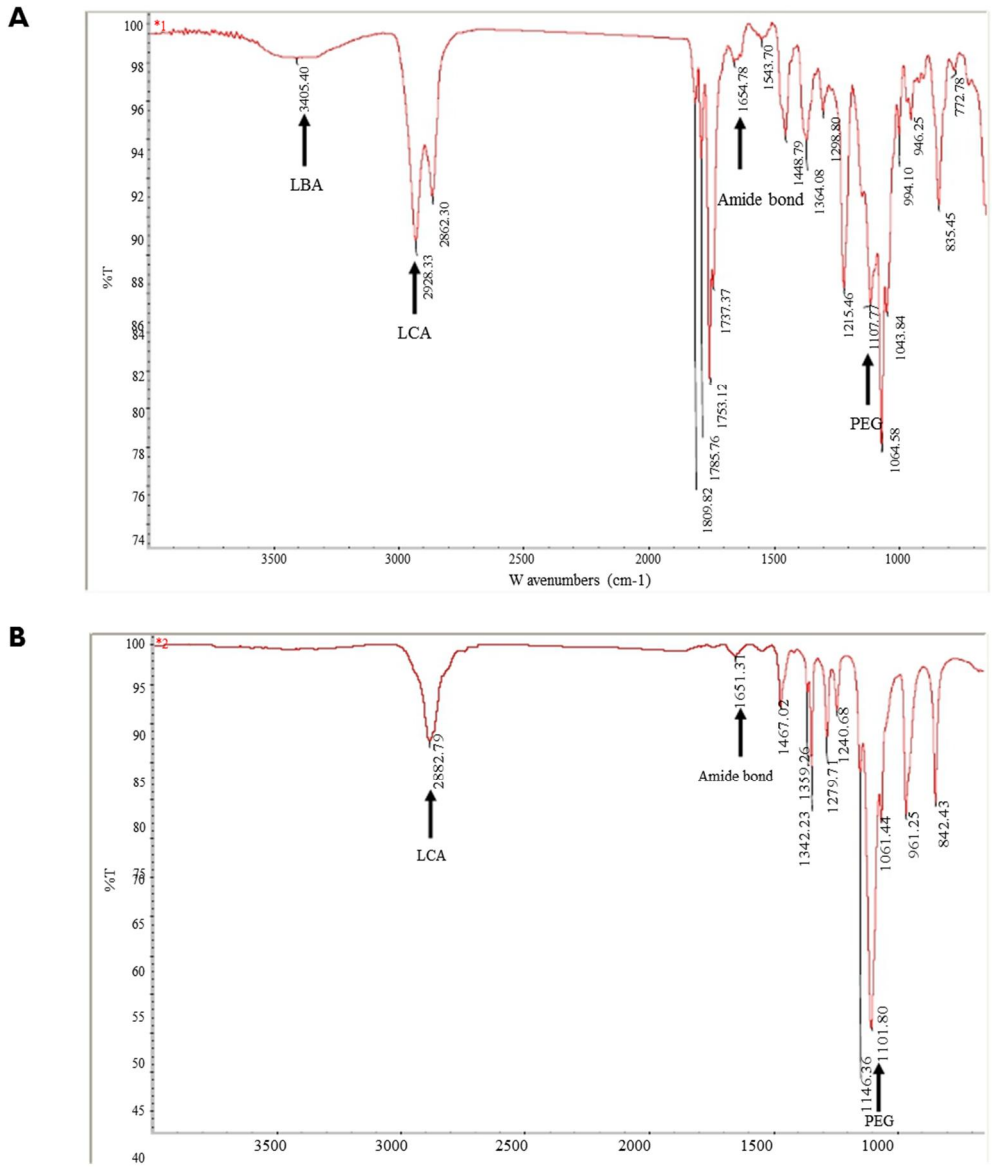

Figure 2. FTIR spectrum of LPL. The characteristic IR peak of LBA, PEG and LCA are indicated by arrowheads.

Figure 3

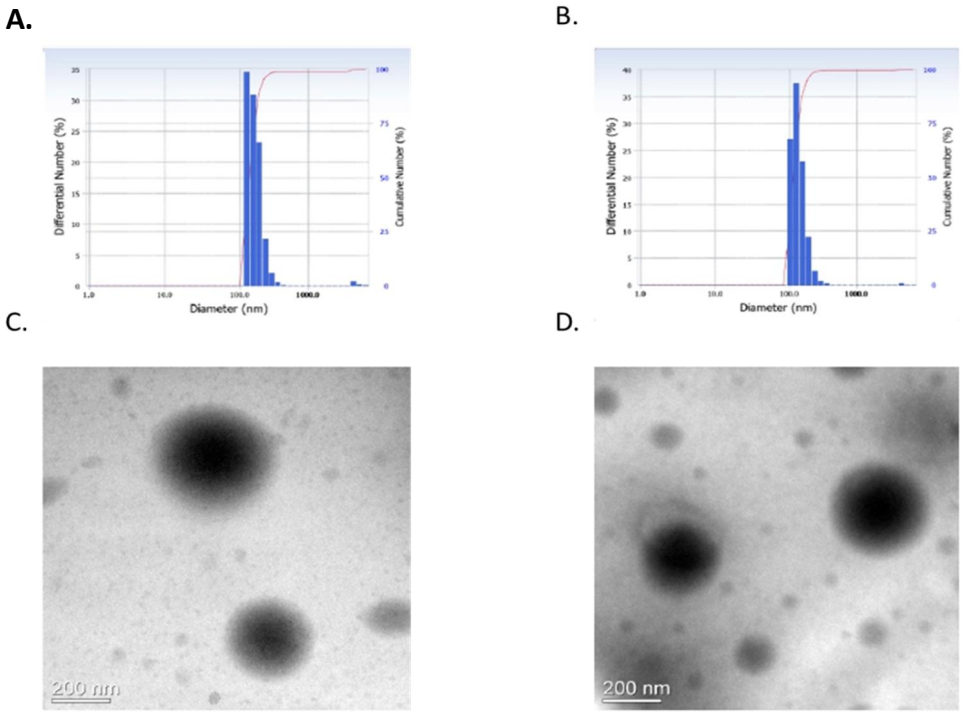

Figure 3. Size and morphology of nanoparticles. The mean hydrodynamic diameter of LPL (A) and PL (B) nanoparticles as measured by DLS. TEM images of LPL (C) and PL nanoparticles (D). Scale Bar = 200 nm.

Figure 4

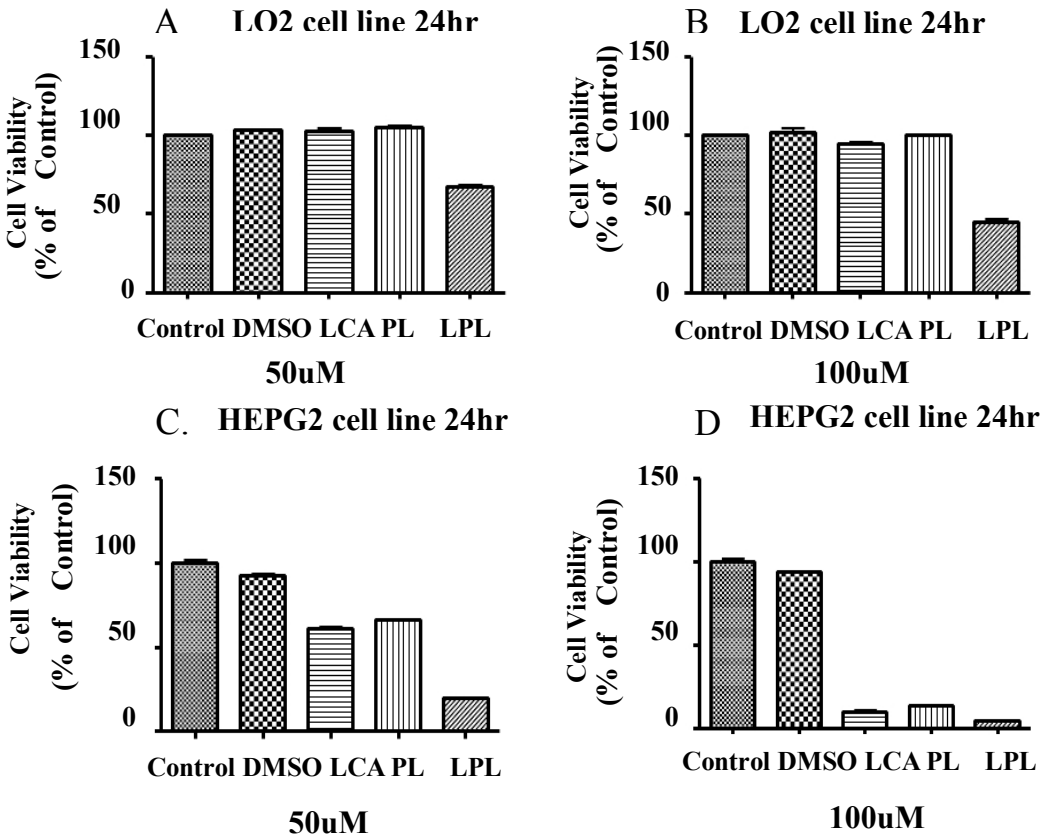

Figure 4. Cell viability test with LPL and PL nanoparticles. LO2 and HepG2 cells were treated with LPL, PL, LCA, DMSO, and untreated group as a control, for 24 h. Cell viability of the cells was analyzed by CCK-8 assay (n=3 independent experiments).

Figure 5

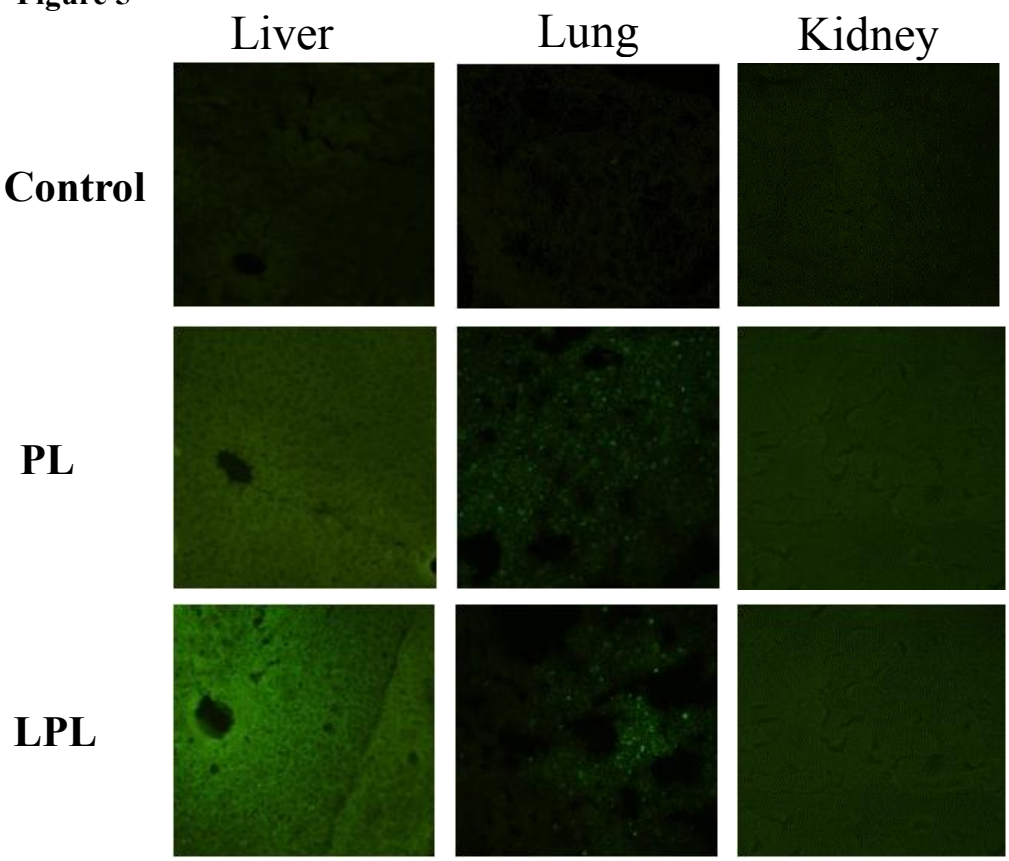

Figure 5. Fluorescent images of tissue sections to detect the cell specificity of LPL and PL nanoparticles. C6-loaded LPL or PL was administered in mice (n=4) by IV injection. After 2 h, the mice were sacrificed and several organs were taken for tissue section to observe the distribution of the nanoparticles.

Figure 6

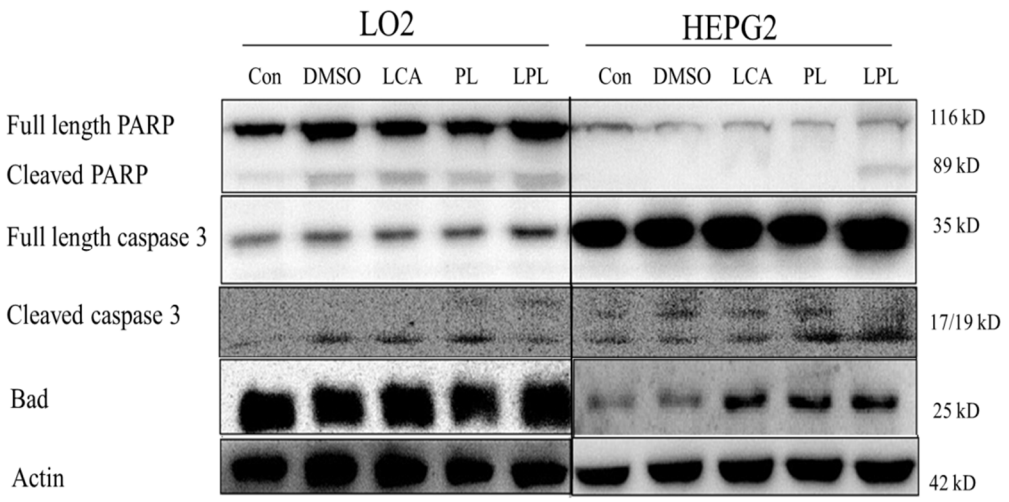

Figure 6. Effects of LPL and PL nanoparticles on the expression of apoptotic proteins in cells. LO2 and HepG2 cells were treated with LPL, PL, LCA, DMSO, and untreated group as a control, for 48 h. Whole-cell lysates were separated by SDS- PAGE and analyzed with specific antibodies on western blot.

Figure 7

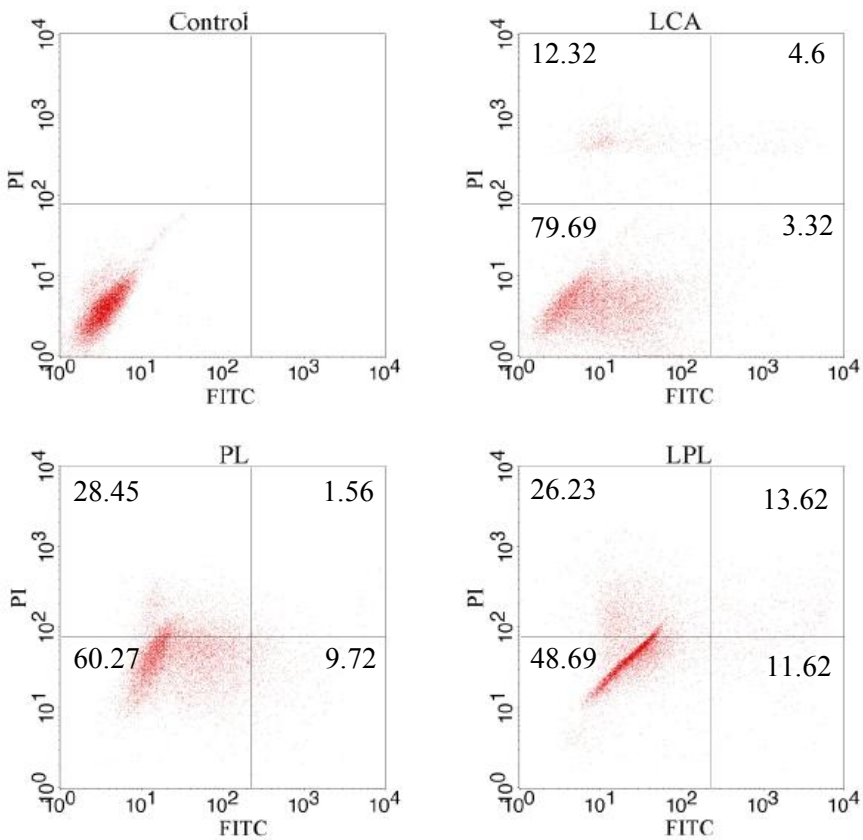

Figure 7. Apoptosis detection by Annexin V-FITC analysis. HepG2 cells were treated with LCA, PL and LPL at concentration of 50 μM for 24 h. Early and late apoptosis are indicated.

Conclusions

In conclusion, we have successfully prepared and evaluated the nanoformulation of LPL for efficient hepatocyte-targeted anti-cancer therapy. Moreover, the nanoparticle formulation of LPL selectively kills liver cancer cells sparing normal liver cells. Current investigations are underway to evaluate the efficacy of anti-cancer drugs-loaded LPL nanoparticles for targeted combinatorial cancer therapy.

Chapter II

Suppression of Tobacco Carcinogen-Induced Lung Tumorigenesis by Aerosol-Delivered Glycerol Propoxylate Triacrylate-Spermine Copolymer/Short Hairpin Rab25 RNA Complexes in Female A/J Mice

(Published in 2016, Journal of Aerosol Medicine and Pulmonary Drug Delivery)

Abstract

Rab25 belongs to the Rab family of small GTPases and is implicated in the development of various types of human cancer including lung cancer that is the leading cause of cancer deaths worldwide. In this study, I report the gene therapeutic effect of small hairpin Rab25 (shRab25) on 4-(Methylnitrosamino)-1-(3-pyridyl)-1-butanone (NNK)-induced lung tumorgenesis in female A/J mice. Initially, six-week-old mice were treated with single dose of NNK (2 mg/0.1 ml saline/mouse) by intraperitonal injection to induce the tumor. eight weeks later, shRab25 was delivered with GPT-SPE complex into tobacco-induced lung cancer models through aerosol delivery. Remarkably, aerosol-delivered shRab25 significantly decreased the expression level of Rab25 and other prominent apoptosis related proteins in female A/J mice. The apoptosis in these mice were determined by detecting the expression level of PCNA, Bcl-2 and Bax, and further confirmed by TUNEL assay. These results strongly support the tumorigenic role of Rab25 in tobacco induced-lung cancer and hence demonstrate aerosol delivery of shRab25 as a promising approach for lung cancer treatment.

Key words: lung cancer, gene therapy, aerosol- deliverered shRab25, NNK, A/J mice

Introduction

Lung cancer is the main cause of cancer-related deaths in the world (1.6 million, 19.4%), and the development of more effective lung cancer therapy still remains challenging (Ferlay et al., 2015). In fact, 80~90% of lung cancers are strongly associated with tobacco smoking. Among the thousands of carcinogenic compounds found in tobacco products, 4-(Methylnitrosamino)-1-(3-pyridyl)-1-butanone (NNK), is the main player to lung carcinogenesis (Akopyan and Bonavida, 2006; Stepanov et al., 2008).

Rab25 belongs to the Rab-related small guanosine triphosphatase (GTPases) proteins; these proteins are considered key regulators of intracellular membrane trafficking involved in various diseases, including cancer (Subramani and Alahari, 2010; Tanos and Rodriguez-Boulan, 2008). Several Rab GTPases, including Rab25, have been examined for being potential drivers in carcinogenesis (Luen Tang, 2010). Studies have shown that Rab25 contributes to the aggressiveness of breast and ovarian cancers (Cheng et al., 2004). Notably, knockdown of Rab25 expression inhibits the growth of ovarian cancer cells (Fan et al., 2006), indicating the essential role for Rab25 in tumor progression and aggressiveness (Agarwal et al., 2009). Specifically, knockdown of Rab25 by siRNA suppressed cell migration and

invasion in non-small-cell lung carcinoma (NSCLC) cells (Ma et al., 2015). While Rab25 expression is positively correlated with E-cadherin, it is negatively associated with ZEB1 in NSCLC cell lines (Roche et al., 2013). Particularly, the effects of Rab25 knockdown on tumor proliferation and apoptosis were confirmed in mice xenografted with gefitinib-sensitive lung cancer cells (Jo et al., 2014).

Many scientists have therefore largely focused on RNA interference (RNAi)-based knock down for cancer therapy. Usually, two kind of RNAi-based therapeutics are well-known: a vector-based short hairpin RNA (shRNA) based on a vector or a chemically synthesized double-stranded small interfering RNA (siRNA)(Rao et al., 2009). A number of studies have been conducted with several RNAi-based therapies, such as shSCRN1 in lung cancer cell lines (Kim et al., 2016), siDDR1in cancer cell lines (Ali-Rahmani et al., 2016), shCul4A in lung cancer cells (Hung et al., 2016) shRab25 in colon cancer cell lines (Krishnan et al., 2013). Comparison with other methods, shRNA has demonstrated great potential as a promising tool for cancer treatment.

Aerosol-mediated gene delivery performs a noninvasive alternative for the targeting of genes to the lungs (Merlin JL, 2001). In this regard, we have previously used several non-viral or viral vectors to transport DNA or siRNA or shRNA through aerosol delivery for lung cancer treatment (Hong

et al., 2015). For example, we delivered shAkt1 by glycerol triacrylate-spermine (GT-SPE) to suppress lung cancer progression (Hong et al., 2012). Similarly, we used polyspermine to deliver Pdcd4 gene that greatly reduced tumor size in K-ras^{LA1} lung cancer model mice (Kim et al., 2014). Also, we have successfully used aerosol delivery of RNAi-based therapeutics by various polymer complexes including spermine-based poly(amino ester)/Akt1shRNA complexes (Jiang et al., 2011), folate–chitosan-graft polyethylenimine/Akt1 shRNA complexes (Jiang et al., 2009), and poly(ester amine)/Akt1 siRNA complexes (Xu et al., 2008). Using lentivirus as a viral vector, several shRNAs, such as AIMP2-DX2 shRNA (Hwang et al., 2013), OPN shRNA (Minai-Tehrani et al., 2013), and PDCD4 shRNA (Hwang et al., 2010) were used for lung cancer treatements through aerosol delivery.

In this study, we delivered short hairpin Rab25 RNA (shRab25) in NNK-induced lung tumorigenesis female A/J mice through aerosol delivery to evaluate the preventive effect of shRab25 in the suppression of lung tumorigenesis.

Materials and methods

Materials

NNK was purchased from Toronto Research Chemicals Inc. (Toronto, Ontario, Canada). Rab25 antibody was purchased from Abcam(Cambridge, UK). α-tubulin Abfrontier (Seoul, Korea), Bax, Bcl-2, proliferating cell nuclear antigen (PCNA) antibodies were purchased from Santa Cruz Biotechnology (Santa Cruz, CA). DeadEND^{TM} Colorimetric TUNEL assay kit was obtained from Promega Corporation (Promega, Madison, WI). Rab25 shRNA (shRab25) and the scrambled control shRNA (shScr) were purchased from Koram Biogen Corp (Korea).

Mouse experiment

Female A/J mice, 5 weeks old, weighing 15-19 g, were received from Central Laboratory Animal Inc. (Seoul, Korea). Mice were housed under standard light/dark cycle at a stable temperature (23°C ± 2°C) and relative humidity (50% ± 10%) in the laboratory animal facility. The mice, 6 weeks of age, were divided into 5 groups, each group containing 8 mice. Four group of mice were injected with single dose of NNK (2 mg/0.1 ml saline/mouse) through intraperitoneal (IP) route. For gene delivery, three groups (except NNK control and saline control group) mice were exposed

with the Rab25 complexes in the nose-only inhalation chamber as described previously (Kim et al., 2004; Tehrani et al., 2007). The polymer complex with DNA (shScr or shRab25) or aerosol containing polymer only were delivered 16 times (twice a week for 8 consequent weeks). Mice were sacrificed one week after exposure and tumor on lung surface were carefully counted, as mentioned previously (Singh et al., 2006). Finally, collected lungs were fixed in 10 % formalin for histopathological examination and remaining lung stored at -70°C for further experiment. All animal experiments were approved by Animal Care and Use Committee at Seoul National University (SNU-140814-3).

Construction of Rab25 shRNA and preparation of GPT–SPE/shRNA complex

The shRNA sequence targeting mouse Rab25 mRNA and scrambled control were purchased. The glycerol propoxylate triacrylate (GPT) - spermine (SPE) copolymer (GPT–SPE) was synthesized as described previously (Jiang et al., 2011). GPT-SPE/shRNA complexes were self-assembled in distilled water by slow adding of 0.8 mg of DNA to 8 mg of polymer solution under gentle mixing. The complexes (final volume 30 ml) were incubated for 30 minutes at room temperature (RT) before delivery.

Western blot analysis

Lung tissues were lysed with IKA® T10 homogenizer (IKA®, Works GmbH & Co, Staufen, Germany) to extract the proteins. Total protein concentration was confirmed by using the Pierce®BCA reagent (Thermo scientific, USA). Equal amounts (25 µg/well) of protein were loaded into 10-12 % SDS-polyacrylamide gels and transferred to nitrocellulose membranes using iBlot system (Life Technologies, Grand Island, NY, USA). Membranes were blocked with Tris-buffered saline with tween 20 (TTBS) containing 5% skim milk for 1 h at RT and immunoblotting was performed by incubation overnight at 4°C with the corresponding primary antibodies. Following day, Antibody labeled with secondary horseradish peroxidase for 4 h at RT. After washing, bands were captured using a model EZ-capture MG luminescent image detector (ATTO, Tokyo, Japan) and analyzed by using ATTO CS Analyzer windows version 3.0 (ATTO, Tokyo, Japan).

Histopathologic and immunohistochemistry analysis

Paraffin-embedded and sectioned lung tissues (4 μm) were stained by hematoxylin and eosin. For immunohistochemistry (IHC) analysis, the lung sections were then deparaffinized in xylene (each for 5 min × 2times) and rehydrated by alcohol gradients (2 min/each), then washed with distilled water and 3% hydrogen peroxide used for 10 min incubation. To block the unspecific binding sites, sections were incubated with 3% bovine serum albumin in TTBS for 1 hour at RT after washing with a TTBS solution. Concerned primary antibodies (1:100) were used overnight at 4°C. Next day, the samples were rinsed by TTBS, and then incubated in secondary antibodies conjugated to horseradish peroxidase (1:200) for 3 hours at RT. Then, 3,3′-diaminobenzidine (DAB) reagent (Life Technologies) was reacted with the tissue sections, those were analyzed by light microscopy. The tissue sections were counterstained with a Mayer's hematoxylin (DAKO, Carpinteria, CA, USA) and mounted using cover slide and the Permount (Fisher Scientific, Waltham, MA). The slides were observed using a Nikon eclipse fluorescence microscopy (Tokyo, Japan).

Analysis of apoptotic cells by TUNEL assay

Determination of apoptotic cells using by DeadEnd^{TM} Colometric tunel assay kit and all steps according to kit's instructions. Briefly, for paraffin-embedded lung tissues sections were deparaffinized and rehydrated by xylene or graded ethanol (100%, 85%, 70% and 50%) at RT, respectively. rTdT reaction mix is added on equilibrated areas and incubated at 37°C for 60 min. After several washes in PBS and 2X SSC, the slides were incubated Streptavidin HRP solution for 30 minutes at RT. For counterstaining procedure, DAB substrate was added to each slide and developed until the appearance of light brown background. Slides were observed by a light microscope to select ×1000 magnification fields (Olympus BX51, Tokyo, Japan).

Statistical analysis

Statistical analysis was performed using analysis of Student's *t*-test with Microcal Origin (Microcal Software, Northampton, USA). Results were expressed as mean values ± standard error of three independent experiments (n=3). All data were compared with corresponding values ($P < 0.001$ was more significant, $P < 0.01$ was highly significant and $P< 0.05$ was considered statistically significant).

Results

In vivo aerosol delivery of shRab25

To determine the carcinogenic function of NNK in vivo, mouse experiment was design as illustrated in Figure 1A. The mice, 6 weeks of age, were divided into 5 groups, each group containing 8 mice. Four group of mice were injected with single dose of NNK (2 mg/0.1 ml saline/mouse) through intraperitoneal (IP) (Takeuchi et al., 2006). Single IP injection of NNK for lung tumorigenesis in A/J mice is a simple procedure that takes 16 weeks for a reasonable yield of lung tumors to develop (Yokohira et al., 2008). The experiment was carried out with one group mice that were treated with an equal volume ofsaline (vehicle control of NNK). Eight weeks later, the NNK-treated mice were exposed with GPT-SPE, GPT-SPE/shScr, GPT-SPE/shRab25 for16 times (twice a week for 8 consequent weeks). Body weights of individual mouse were recorded weekly for 8 weeks during the aerosol delivery (Figure 1B).

Aerosol delivery of Rab25 shRNA suppresses tumorigenesis in lung

As shown in Fig. 2A, the injection of NNK induced number of tumors in lungs while there was no such tumor growth in lungs of control group mice (saline). After aerosol delivery of GPT-SPE, GPT-SPE/shScr, GPT-SPE/shRab25 in NNK-induced A/J mice for 8 weeks, we found that GPT-SPE/shRab25 largely decreased the tobacco-induced tumor numbers in the lungs in compared to GPT-SPE or GPT-SPE/shScr delivered groups. The observable antitumor effects of GPT-SPE/shRab25 were illustrated with graph (Figure 2 B, C and Table 1). The results showed that aerosol-delivered GPT-SPE/shRab25 complex significantly decreased lung tumor number (n=5) (Figure 2B) and tumor volume (n=5) (Figure 2C). For further confirmation of anti-tumor effect of aerosol-delivered GPT-SPE/shRab25 complex, we performed the histopathologic analysis of lung tissues of mice 8 weeks after the aerosol delivery (Figure 2D). The results demonstrated the higher tumor suppression effect of GPT-SPE/shRab25 than other GPT-SPE or GPT-SPE/shScr treated groups.

Cell proliferation was suppressed in Aerosol delivery of shRab25

To evaluate cell proliferation in tumor tissue, IHC and western blot studies were performed. Western blot results confirmed that aerosol-delivered GPT-SPE/shRab25 group had very low level of PCNA expression than GPT-SPE or GPT-SPE/shScr groups (Figure 3A). Further densitometry analyses revealed that the expression level of PCNA in GPT-SPE/shRab25 group was significantly lower than other groups (Figure 3B). We also investigated the expression level of PCNA by IHC. The experimental results demonstrated the clear evidence of lower expression of PCNA in GPT-SPE/shRab25 group (Figure 3C). In addition, PCNA counting analysis showed that delivery of GPT-SPE/shRab25 significantly decreased PCNA positive cells compared to the NNK control, NNK+GPT-SPE only, and NNK+GPT-SPE/shScr group (Figure 3D).

Down-regulation of Rab25 induced apoptotic cell death in lung cancer

To determine the expression level of Rab25 in theA/J mice lungs of NNK treated A/J mice after inhalation of shRab25, western blot analysis was accomplished. Western blot result clearly demonstrated that the expression

level of Rab25 after inhalation of GPT-SPE/shRab25 in the NNK induced A/J mice largely decreased when compared to only NNK-treated A/J mice (Figure 4A). Quantification of the western blot further confirmed the low expression of Rab25 in GPT-SPE/shRab25 delivered group (n=3, $P<0.05$ compared with NNK control) (Figure 4B). To corroborate the induction of apoptosis by aerosol delivery of GPT-SPE/shRab25, we investigated the expressions of Bax (a pro-apoptotic protein) and Bcl-2 (an anti-apoptotic protein) proteins in lung tissues by western blots. The results showed that the level of Bcl-2 decreased significantly in the GPT-SPE/shRab25 delivered group (n=3) than other controls. In contrast, the level of Bax increased in the GPT-SPE/shRab25 delivered group (n=3) than other groups (Figure 4C and 4E). Further, detection of apoptosis by TUNEL assay also indicated the higher amount of TUNEL-positive cells in the the NNK+GPT-SPE/shRab25 group (Figure 4 F).

Figure 1

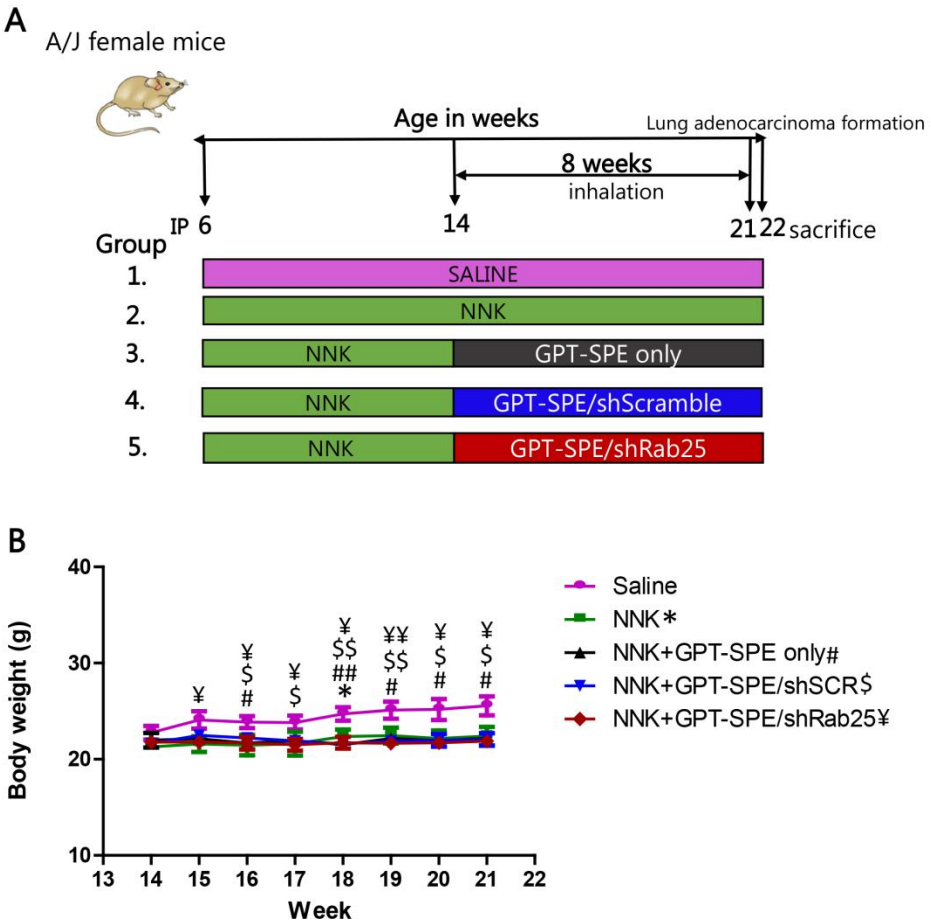

Figure 1. (A) Experimental design of tumor induction and treatment. Six-week-old mice (eight mice/group) were injected intraperitoneally with NNK(100mg/kg). At 22 weeks, mice were sacrificed and lungs were harvested for evaluation of lung tumors. (B) Body weight of mice from 14 to 21 weeks during aerosol delivery ($n = 5$, $^{*}p < 0.05$ saline compared to

NNK+GPT-SPE only, NNK+GPT-SPE/shScr, and NNK+GPT-SPE/shRab25). GPT-SPE glycerol propoxylate triacrylate-spermine; shRab25, short hairpin Rab25 RNA.

Figure 2

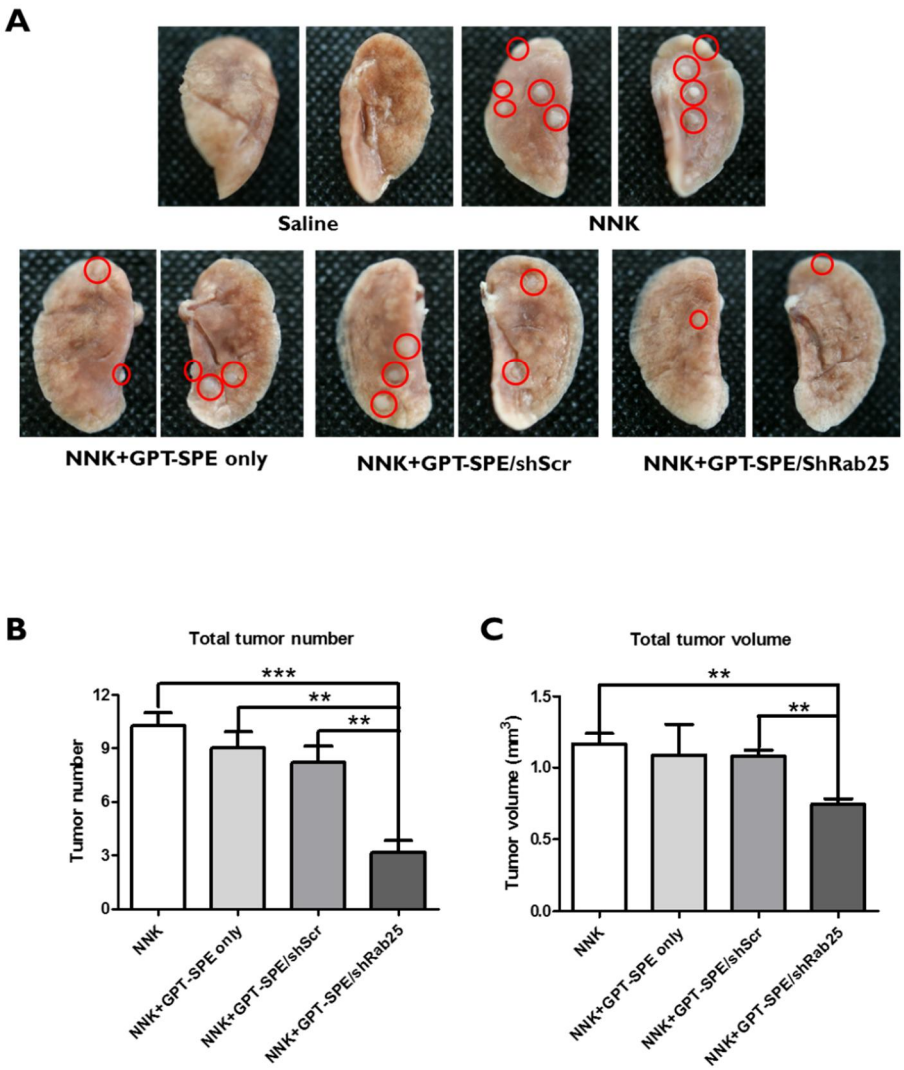

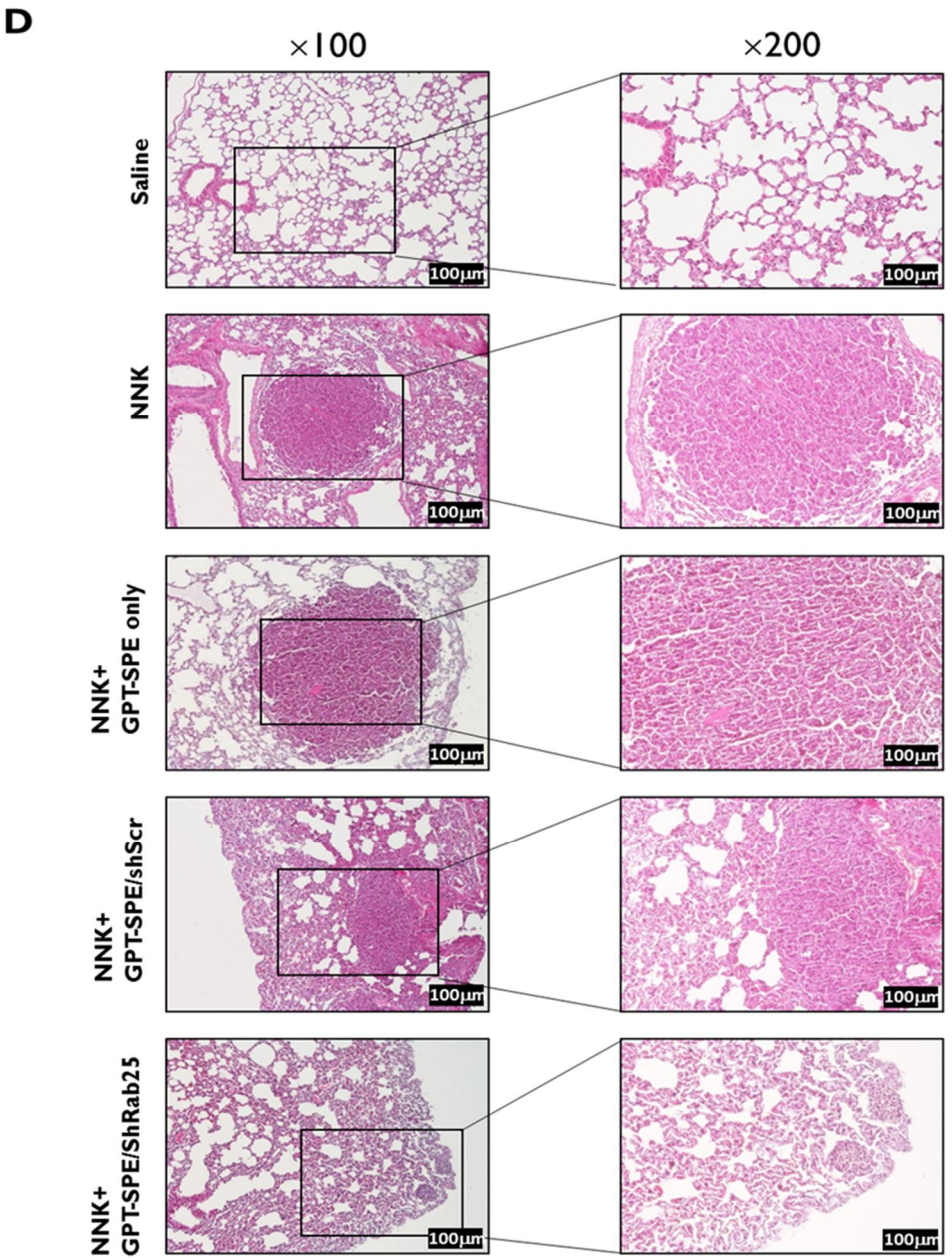

Figure 2. Therapeutic efficiency of shRab25 through aerosol delivery in A/J mice. Therapeutic efficiency of shRab25 through aerosol delivery in A/J mice. (A) Lung tumor lesions. (B) Total tumor numbers ($n = 5$, $^{***}p < 0.001$

compared to NNK control, $^{**}p < 0.01$ compared to NNK+GPT-SPE only and NNK+GPT-SPE/shScr). (C) Total tumor volume ($^{**}p < 0.01$ compared to NNK control and NNK+GPT-SPE/shScr). (D) Histopathological features (magnification, 100×and 200×).

Figure 3

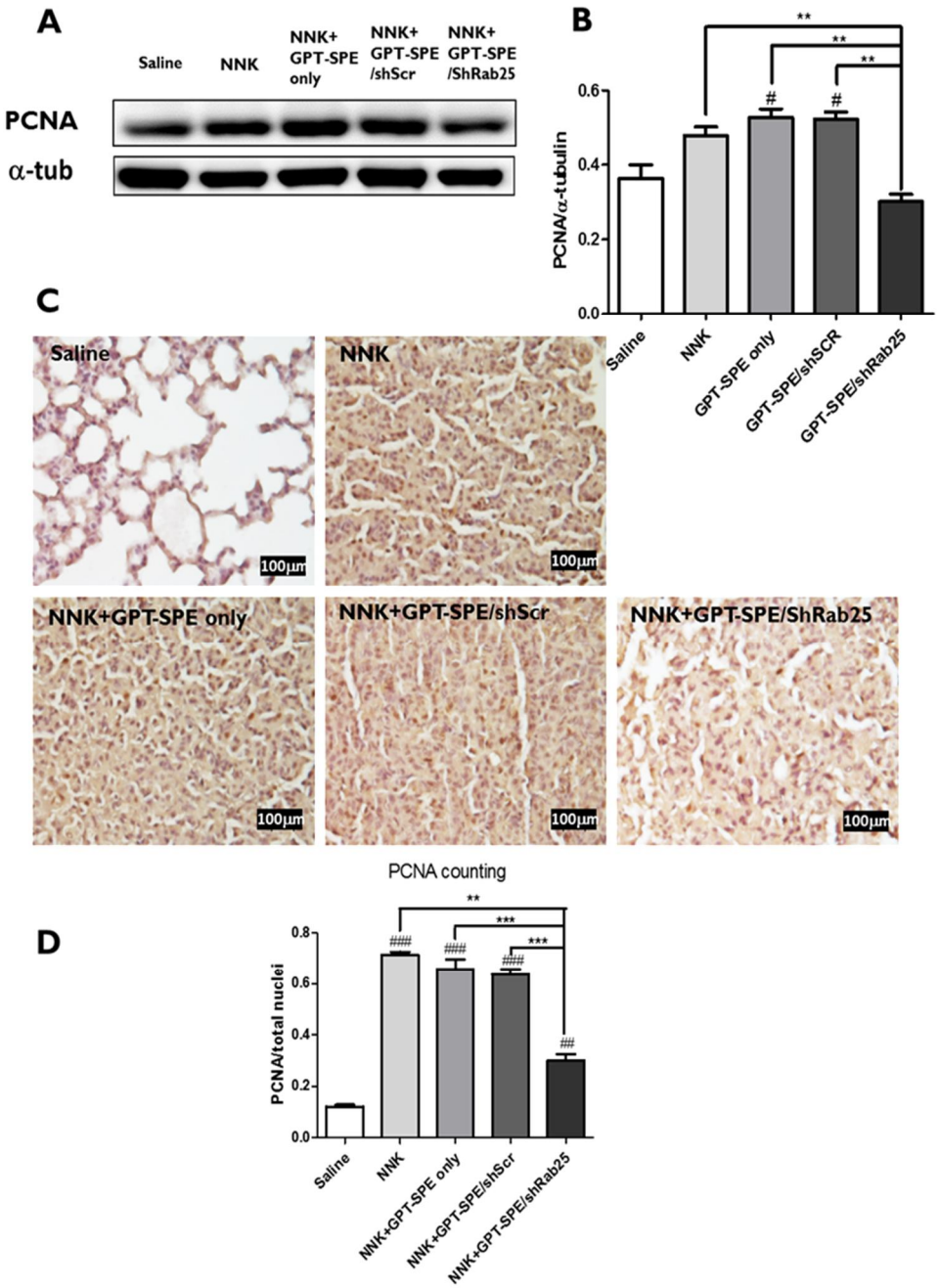
A
Saline
NNK
NNK+ GPT-SPE only
NNK+ GPT-SPE /shScr
NNK+ GPT-SPE /ShRab25
PCNA
α-tub
B
PCNA/α-tubulin
0.0
0.2
0.4
0.6
**
**
**
#
#
Saline
NNK
GPT-SPE only
GPT-SPE/shSCR
GPT-SPE/shRab25
C
Saline
NNK
NNK+GPT-SPE only
NNK+GPT-SPE/shScr
NNK+GPT-SPE/ShRab25
100μm
D
PCNA counting
PCNA/total nuclei
0.0
0.2
0.4
0.6
0.8
**
***
***
###
###
###
##
Saline
NNK
NNK+GPT-SPE only
NNK+GPT-SPE/shScr
NNK+GPT-SPE/shRab25

Figure 3. Inhibition of cell proliferation by aerosol delivery of shRab25. (A) Western blot analysis of PCNA. (B) Quantification of PCNA expression. Bands were analyzed by densitometer ($n = 3$, $^{**}p < 0.01$ compared to NNK control, NNK+GPT-SPE only, and NNK+GPT-SPE/shScr. $^{\#}p < 0.05$ compared to saline control).

(C) PCNA immunohistochemistry analysis (magnification, 400×). (D) PCNA counting ($n = 3$, $^{**}p < 0.01$compared to NNK control, $^{***}p < 0.001$ compared GPT-SPE only and GPT-SPE/shScr, $^{\#\#\#}p < 0.001$ compared to saline control, $^{\#\#}p < 0.01$ compared to saline control). PCNA, proliferating cell nuclear antigen.

Figure 4

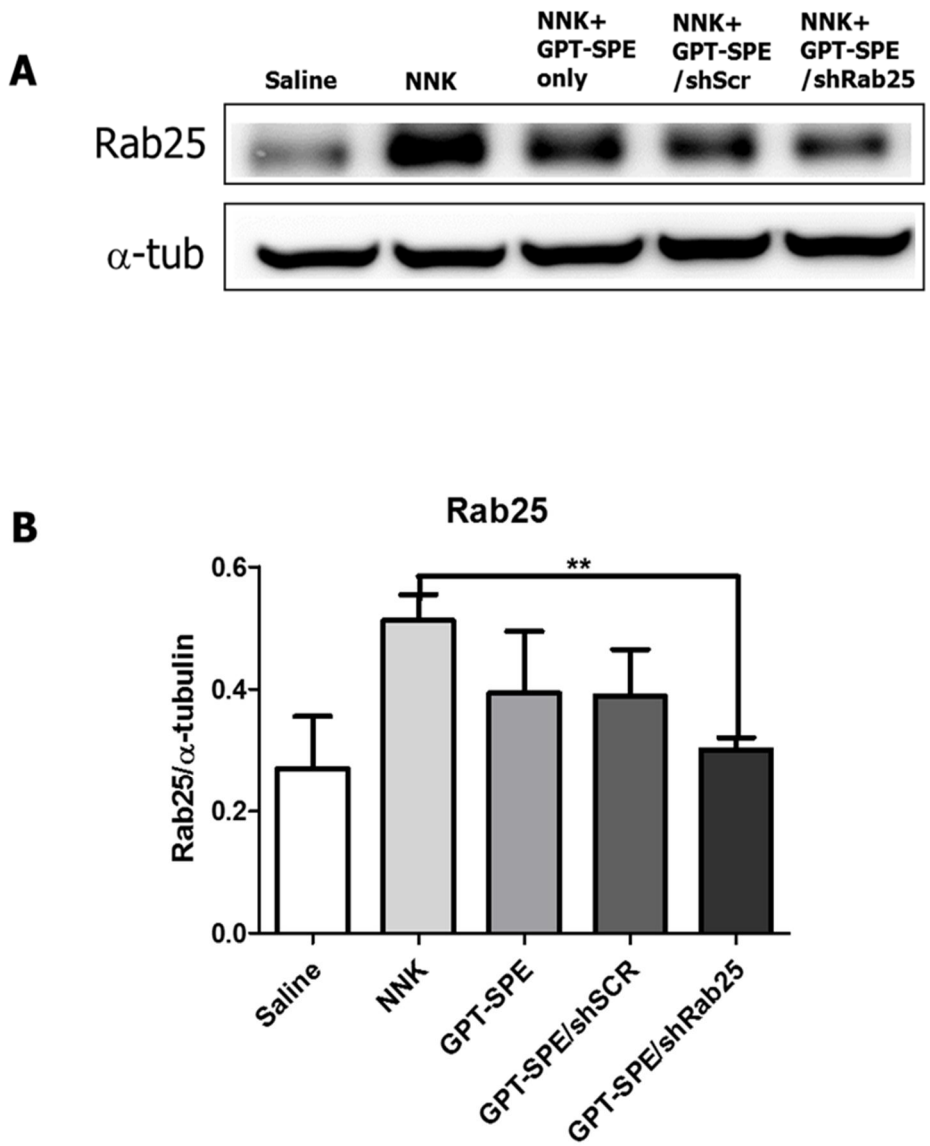
A
Saline
NNK
NNK+ GPT-SPE only
NNK+ GPT-SPE /shScr
NNK+ GPT-SPE /shRab25
Rab25
α-tub
B
Rab25
**
Rab25/α-tubulin
0.6
0.4
0.2
0.0
Saline
NNK
GPT-SPE
GPT-SPE/shSCR
GPT-SPE/shRab25

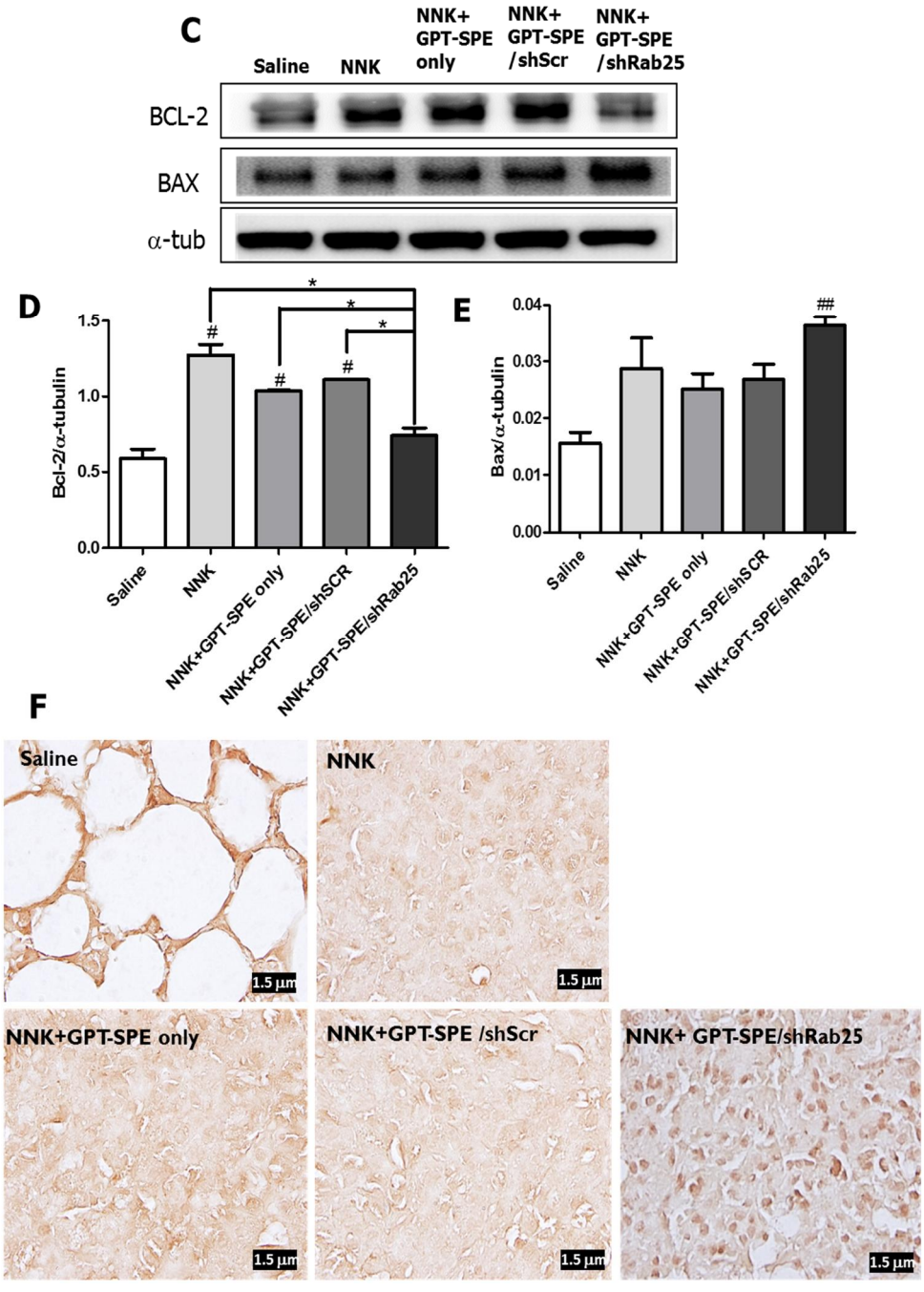
C
Saline
NNK
NNK+ GPT-SPE only
NNK+ GPT-SPE /shScr
NNK+ GPT-SPE /shRab25
BCL-2
BAX
α-tub
D
Bcl-2/α-tubulin
1.5
1.0
0.5
0.0
Saline
NNK
NNK+GPT-SPE only
NNK+GPT-SPE/shSCR
NNK+GPT-SPE/shRab25
E
Bax/α-tubulin
0.04
0.03
0.02
0.01
0.00
F
Saline
NNK
NNK+GPT-SPE only
NNK+GPT-SPE /shScr
NNK+ GPT-SPE/shRab25
1.5 μm

Figure 4. Determination of apoptosis mechanism by aerosol delivery of shRab25. (A, C) Western blot analysis. Statistical analysis of western blot (B) Rab25 ($n = 3$, $^{**}p < 0.01$ compared to NNK control). (D) Bcl-2 ($n = 3$, $^{*}p < 0.05$ compared to NNK control, NNK+GPT-SPE only, NNK+GPT-SPE/shScr, $^{\#}p<0.05$ compared to saline control). (E) Bax ($n = 3$, $^{\#\#}p<0.01$ compared to saline control). (F) Colorimetric TUNEL assay.

Table 1

Group	Mice identification	No.of Adenocarcinoma	No.of Adenoma	No.of hyperplasia foci
NNK control	1	4	2	1
	2	4	1	1
	3	2	1	3
	4	3.33	0	0
	5	3.5	3	3
Avg		**3.36**	**1.4**	**1.6**
STD		0.82	1.14	1.34
NNK+GPT-SPE only	1	1	0	2
	2	3	1	2
	3	3	1	0
	4	4	2	3
	5	3	1	2
Avg		**2.8**	**1**	**1.8**
STD		1.10	0.71	1.10
NNK+GPT-SPE/shScramble	1	3	1	1
	2	3	1	2
	3	3.5	1	2
	4	3	0	2
	5	3	2	3
Avg		**3.1**	**1**	**2**
STD		0.22	0.71	0.63
NNK+GPT-SPE/ShRab25	1	1	1	2
	2	2	0	0
	3	2	2	2
	4	1	0	3
	5	1	0	0
Avg		**1.4** **,#,$$$	**0.6**	**1.4**
STD		0.55	0.89	1.34

Table 1. Summary of tumor incidence in NNK treated A/J mice

** $p < 0.01$ compared to NNK group, # $p < 0.05$ compared to GPT-SPE only, $$$ $p < 0.001$ compared to GPT-SPE/shScr. GPT-SPE, glycerol propoxylate triacrylate-spermine; NNK only, mice induced with NNK as a positive control; NNK+GTP-SPE only, mice induced with NNK and treated with GPT-SPE copolymer; NNK+GTP-SPE/shScr, mice induced with NNK and treated with GPTSPE/shScr complex; NNK+GTP-SPE/shRab25, mice induced with NNK and treated with GPT-SPE/shRab25 complex; shRab25, short hairpin Rab25 RNA; STD, standard deviation

Discussion

Rab25 signaling pathway plays a role in the regulation of cell proliferation and apoptosis in cancer cells indicating that the Rab25 gene plays an important role in tumor occurrence and development (Agola et al., 2011). Previous *in vitro* studies referred that down-regulation of Rab25 has large effect on cancer suppression and indicated that Rab25 could be an essential molecular target for cancer therapy (Amornphimoltham et al., 2013; Tong et al., 2012; Zhang et al., 2013). Considering gene therapy as a promising treatment strategy for cancer, aerosol delivery of therapeutic genes seems the most convenient way for lung cancer gene therapy because it is simple, non-invasive and direct method that makes instant access to lungs without any effect to other organs due to the anatomical structure and location of the lungs inside the body (Gautam et al., 2003). Besides, the large surface area, good vascularization, and ultra-thin structure of the alveolar epithelium are distinctive features of the lung that can facilitate systemic delivery via pulmonary route (Uchenna Agu et al., 2001). Moreover, aerosol particles can reach the gas-exchange surfaces of the alveolar region of the lung (Theunissen R, 2008), rendering the pulmonary route as an attractive pathway for aerosol delivery. Recently, aerosol delivery of polyethyleneimine (PEI) complexes of p53 and IL-12 genes stimulated

higher therapeutic responses in different animal lung tumor models (Gautam et al., 2001; Gautam et al., 2003). PEI forms stable complexation with DNA to protect DNA from degradation and stable during nebulization. Although PEI has been known to be an efficient vector for gene delivery both in vitro and in vivo, it exerts some degree of cytotoxicity when administered to body.

In pursuit of low toxic gene carrier, researchers have made a number of polymers based on PEI backbone to reduce the cytotoxic property of gene carrier. In fact, spermine-based poly(amino ester)/DNA complexes are less toxic than PEI 25K based complexes. In this study, we therefore used spermine, a short homologue of PEI, in combination with glycerol to prepare a biodegradable copolymer (GPT-SPE) as a gene delivery carrier. Particularly, GPT–SPE had low cytotoxicity and it exhibited high ability to form complex with DNA. Besides, the physicochemical and biological characterizations of GPT–SPE exhibited it as a safe and efficient gene delivery carrier. Consequently, GPT–SPE efficiently delivered shRNA through aerosol route for lung cancer gene therapy (Jiang et al., 2011). Since the properties of GPT–SPE deemed safe and efficient, we selected GPT–SPE to deliver DNA, especially shRNA to downregulate Rab25 in lung cancer through RNAi mechanism.

Fortunately, the emergence of RNAi phenomenon has provided new opportunities for cancer therapy. Particularly, shRNAs that enable persistent suppression of sequence-specific gene silencing show great promise for therapeutic applications. Accordingly, our research group have used various polymers to deliver Akt1 shRNAs (shAkt1) by aerosol route for in vivo lung cancer therapy. For example, we used folate–chitosan-graft-PEI to deliver shAkt1to suppress the lung tumorigenesis in male A/J mice (Jiang et al., 2009). In another study, GT-SPE/shAkt1complex suppressed lung tumorigenesis in a K-ras^{LA1} lung cancer mice model by inducing apoptosis through the Akt signaling pathway and cell cycle arrest (Hong et al., 2012). Similarly, aerosol delivery of GPT–SPE/shAkt1complexes greatly suppressed lung tumorigenesis in K-ras^{LA1} lung cancer model mice (Jiang et al., 2011).

Considering that apoptosis induction by shRNA would be an efficient and promising strategy for cancer gene therapy, we determined to evaluate the effect of Rab25 shRNA in lung tumorigenesis through aerosol delivery. Importantly, downregulation of Rab25 by shRNA exhibited proliferation, induced apoptotic cell death, and then decreased tumor growth in ovarian cancer xenograft mouse (Fan et al., 2006). In this study, we used female A/J mice to observe *in vivo* effects of aerosol-delivered Rab25 shRNA in lung tumorigenesis because female A/J mice are more sensitive to NNK-induced

lung carcinogenesis than males (Igarashi et al., 2009). We took advantage of our potent gene carrier, GPT-SPE, to deliver shRNA for lung tumor therapy. As expected, aerosol delivery of GPT-SPE/shRab25 complexes in the female A/J mice showed remarkable anticancer effects. The total tumor number and tumor volume of lung surface neoplastic lesions were significantly decreased after repeated aerosol delivery of shRab25. Similarly, the nodules (adenocarcinoma and adenoma) and their numbers were comparably smaller in the lungs of NNK+GPT-SPE/shRab25 treated mice group than in the lungs of mice treated with NNK control, NNK+GPT-SPE/shScr and NNK+GPT-SPE only groups (Table 1).

Notably, the aerosol delivery of GPT-SPE/shRab25 largely decreased the PCNA expression levels, as detected by IHC and Western blot. PCNA protein plays great role in the process of life and death of the cell. Usually apoptosis occurs, when PCNA is absent or present in low quantities in the cell (Paunesku et al., 2001). Consistently, aerosol-delivered GPT-SPE/shRab25 decreased Rab25 expression levels as examined by densitometric analysis and western blot. Besides, our *in vivo* study revealed that GPT-SPE/shRab25 induced apoptotic cell death, associated with Bcl-2 downregulation and Bax upregulation, which is a well known phenomemon of a mitochondria-mediated apoptosis pathway where Bax is translocated to mitochondia from cytosol through the reduction of Bcl-2. To further assess

the suppression of lung cancer progression by shRab25 is associated with apoptosis proteins, we performed TUNEL assay to detect the abundance of apoptosis-related proteins in the lung tissues. The TUNEL assay confirmed the higher number of TUNEL-positive cells in the NNK+GPT-SPE/shRab25 group than other controls. These data exhibited that shRab25 could facilitate apoptosis in the lungs of NNK-induced A/J mice.

In summary, the present investigation demonstrated that aerosol delivery of shRab25 complex efficiently suppressed the tobacco carcinogen-induced lung cancer. Thus, this study confirmed that the aerosol delivery system could offer a promising approach for specific delivery of shRNA as an effective tobacco carcinogen-induced lung cancer therapy. To our best knowledge, this study is the first demonstration of the treatment of tobacco carcinogen-induced lung tumorigenesis in A/J mice by using Rab25 shRNA.

References

Agarwal, R., Jurisica, I., Mills, G.B., Cheng, K.W., 2009. The emerging role of the RAB25 small GTPase in cancer. Traffic 10, 1561-1568.

Agola, J.O., Jim, P.A., Ward, H.H., BasuRay, S., Wandinger-Ness, A., 2011. Rab GTPases as regulators of endocytosis, targets of disease and therapeutic opportunities. Clinical Genetics 80, 305-318.

Akopyan, G., Bonavida, B., 2006. Understanding tobacco smoke carcinogen NNK and lung tumorigenesis. International journal of oncology 29, 745-752.

Ali-Rahmani, F., FitzGerald, D.J., Martin, S., Patel, P., Prunotto, M., Ormanoglu, P., Thomas, C., Pastan, I., 2016. Anticancer Effects of Mesothelin-Targeted Immunotoxin Therapy Are Regulated by Tyrosine Kinase DDR1. Cancer Res 76, 1560-1568.

Amornphimoltham, P., Rechache, K., Thompson, J., Masedunskas, A., Leelahavanichkul, K., Patel, V., Molinolo, A., Gutkind, J.S., Weigert, R., 2013. Rab25 regulates invasion and metastasis in head and neck cancer. Clinical cancer research : an official journal of the American Association for Cancer Research 19, 1375-1388.

Chaffer, C.L., Weinberg, R.A., 2011. A perspective on cancer cell metastasis. Science 331, 1559-1564.

Cheng, K.W., Lahad, J.P., Kuo, W.-l., Lapuk, A., Yamada, K., Auersperg, N., Liu, J., Smith-McCune, K., Lu, K.H., Fishman, D., Gray, J.W., Mills, G.B., 2004. The RAB25 small GTPase determines aggressiveness of ovarian and breast cancers. Nat Med 10, 1251-1256.

Cordeiro, R.A., Santo, D., Farinha, D., Serra, A., Faneca, H., Coelho, J.F.J., High transfection efficiency promoted by tailor-made cationic tri-block copolymer-based nanoparticles. Acta Biomaterialia.

Cu, Y., Saltzman, W.M., 2009. Controlled Surface Modification with Poly(ethylene)glycol Enhances Diffusion of PLGA Nanoparticles in Human Cervical Mucus. Molecular Pharmaceutics 6, 173-181.

D'Souza, A.J.M., Topp, E.M., 2004. Release from polymeric prodrugs: Linkages and their degradation. Journal of Pharmaceutical Sciences 93, 1962-1979.

Du, Q., Zhang, Y., Pan, Y., Duan, T., 2014. Lithocholic acid-induced placental tumor necrosis factor-α upregulation and syncytiotrophoblast cell apoptosis in intrahepatic cholestasis of pregnancy. Hepatology Research 44, 532-541.

Duncan, R., 2006. Polymer conjugates as anticancer nanomedicines. Nature reviews Cancer 6, 688-701.

Fan, Y., Xin, X.Y., Chen, B.L., Ma, X., 2006. Knockdown of RAB25 expression by RNAi inhibits growth of human epithelial ovarian cancer cells in vitro and in vivo. Pathology 38, 561-567.

Ferlay, J., Soerjomataram, I., Dikshit, R., Eser, S., Mathers, C., Rebelo, M., Parkin, D.M., Forman, D., Bray, F., 2015. Cancer incidence and mortality worldwide: Sources, methods and major patterns in GLOBOCAN 2012. International journal of cancer 136, E359-E386.

Gautam, A., Densmore, C.L., Waldrep, J.C., 2001. Pulmonary cytokine responses associated with PEI-DNA aerosol gene therapy. Gene therapy 8, 254-257.

Gautam, A., Waldrep, J.C., Densmore, C.L., 2003. Aerosol gene therapy. Molecular biotechnology 23, 51-60.

Goldberg, A.A., Beach, A., Davies, G.F., Harkness, T.A.A., LeBlanc, A., Titorenko, V.I., 2011. Lithocholic bile acid selectively kills neuroblastoma cells, while sparing normal neuronal cells.

Goldberg, A.A., Titorenko, V.I., Beach, A., Sanderson, J.T., 2013. Bile acids induce apoptosis selectively in androgen-dependent and -independent prostate cancer cells. PeerJ 1, e122.

Harris, J.M., Chess, R.B., 2003. Effect of pegylation on pharmaceuticals. Nat Rev Drug Discov 2, 214-221.

Hecht, S.S., Morse, M.A., Amin, S., Stoner, G.D., Jordan, K.G., Choi, C.-I., Chung, F.-L., 1989. Rapid single-dose model for lung tumor induction in A/J mice by 4-(methylnitrosainino)-1-(3-pyridyl)-1-butanone and the effect of diet. Carcinogenesis 10, 1901-1904.

Hong, S.-H., Park, S.-J., Lee, S., Cho, C.S., Cho, M.-H., 2015. Aerosol gene delivery using viral vectors and cationic carriers for in vivo lung cancer therapy. Expert Opinion on Drug Delivery 12, 977-991.

Hong, S.H., Kim, J.E., Kim, Y.K., Minai-Tehrani, A., Shin, J.Y., Kang, B., Kim, H.J., Cho, C.S., Chae, C., Jiang, H.L., Cho, M.H., 2012. Suppression of lung cancer progression by biocompatible glycerol triacrylate-spermine-mediated delivery of shAkt1. International journal of nanomedicine 7, 2293-2306.

Hung, M.S., Chen, I.C., You, L., Jablons, D.M., Li, Y.C., Mao, J.H., Xu, Z., Lung, J.H., Yang, C.T., Liu, S.T., 2016. Knockdown of cullin 4A inhibits growth and increases chemosensitivity in lung cancer cells. Journal of Cellular and Molecular Medicine 20, 1295-1306.

Hwang, S.K., Chang, S.H., Minai-Tehrani, A., Kim, Y.S., Cho, M.H., 2013. Lentivirus-AIMP2-DX2 shRNA suppresses cell proliferation by regulating Akt1 signaling

pathway in the lungs of AIMP2(+)/(-) mice. Journal of aerosol medicine and pulmonary drug delivery 26, 165-173.

Hwang, S.K., Minai-Tehrani, A., Lim, H.T., Shin, J.Y., An, G.H., Lee, K.H., Park, K.R., Kim, Y.S., Beck, G.R., Jr., Yang, H.S., Cho, M.H., 2010. Decreased level of PDCD4 (programmed cell death 4) protein activated cell proliferation in the lung of A/J mouse. Journal of aerosol medicine and pulmonary drug delivery 23, 285-293.

Igarashi, M., Watanabe, M., Yoshida, M., Sugaya, K., Endo, Y., Miyajima, N., Abe, M., Sugano, S., Nakae, D., 2009. Enhancement of lung carcinogenesis initiated with 4-(N-hydroxymethylnitrosamino)-1-(3-pyridyl)-1-butanone by Ogg1 gene deficiency in female, but not male, mice. The Journal of Toxicological Sciences 34, 163-174.

Izunobi J. U. , H.C.L., 2011. Polymer Molecular Weight Analysis by 1H Nuclear Magnetic Resonance Spectroscopy. J Chem Educ 88, 1098.

Jemal, A., Siegel, R., Ward, E., Hao, Y., Xu, J., Murray, T., Thun, M.J., 2008. Cancer Statistics, 2008. CA: a cancer journal for clinicians 58, 71-96.

Jiang, H.-L., Hong, S.-H., Kim, Y.-K., Islam, M.A., Kim, H.-J., Choi, Y.-J., Nah, J.-W., Lee, K.-H., Han, K.-W., Chae, C., Cho, C.-S., Cho, M.-H., 2011. Aerosol delivery of spermine-based poly(amino ester)/Akt1 shRNA complexes for lung cancer gene therapy. International Journal of Pharmaceutics 420, 256-265.

Jiang, H.-L., Xu, C.-X., Kim, Y.-K., Arote, R., Jere, D., Lim, H.-T., Cho, M.-H., Cho, C.-S., 2009. The suppression of lung tumorigenesis by aerosol-delivered folate–chitosan-graft-polyethylenimine/Akt1 shRNA complexes through the Akt signaling pathway. Biomaterials 30, 5844-5852.

Jo, U., Park, K.H., Whang, Y.M., Sung, J.S., Won, N.H., Park, J.K., Kim, Y.H., 2014. EGFR endocytosis is a novel therapeutic target in lung cancer with wild-type EGFR. Oncotarget 5, 1265-1278.

Katona, B.W., Anant, S., Covey, D.F., Stenson, W.F., 2009. Characterization of Enantiomeric Bile Acid-induced Apoptosis in Colon Cancer Cell Lines. The Journal of biological chemistry 284, 3354-3364.

Kim, H.W., Park, I.K., Cho, C.S., Lee, K.H., Beck, G.R., Jr., Colburn, N.H., Cho, M.H., 2004. Aerosol delivery of glucosylated polyethylenimine/phosphatase and tensin homologue deleted on chromosome 10 complex suppresses Akt downstream pathways in the lung of K-ras null mice. Cancer Res 64, 7971-7976.

Kim, N., Cho, A., Watanabe, H., Choi, Y.-L., Aziz, M., Kassner, M., Joung, J.-G., Park, A.K.J., Francis, J.M., Bae, J.S., Ahn, S.-m., Kim, K.-M., Park, J.O., Park, W.-Y., Ahn, M.-J., Park, K., Koo, J., Yin, H.H., Cho, J., 2016. Integrated genomic approaches identify upregulation of SCRN1 as a novel mechanism associated with acquired resistance to erlotinib in PC9 cells harboring oncogenic EGFR mutation. Oncotarget 7, 13797-13809.

Kim, Y.-K., Cho, C.-S., Cho, M.-H., Jiang, H.-L., 2014. Spermine-alt-poly(ethylene glycol) polyspermine as a safe and efficient aerosol gene carrier for lung cancer therapy. Journal of Biomedical Materials Research Part A 102, 2230-2237.

Kitada, S., Krajewska, M., Zhang, X., Scudiero, D., Zapata, J.M., Wang, H.G., Shabaik, A., Tudor, G., Krajewski, S., Myers, T.G., Johnson, G.S., Sausville, E.A., Reed, J.C., 1998. Expression and location of pro-apoptotic Bcl-2 family protein BAD in normal human tissues and tumor cell lines. The American journal of pathology 152, 51-61.

Kozoni, V., Tsioulias, G., Shiff, S., Rigas, B., 2000. The effect of lithocholic acid on proliferation and apoptosis during the early stages of colon carcinogenesis: differential effect on apoptosis in the presence of a colon carcinogen. Carcinogenesis 21, 999-1005.

Krishnakumar, R., Kraus, W.L., 2010. The PARP Side of the Nucleus: Molecular Actions, Physiological Outcomes, and Clinical Targets. Molecular Cell 39, 8-24.

Krishnan, M., Lapierre, L.A., Knowles, B.C., Goldenring, J.R., 2013. Rab25 regulates integrin expression in polarized colonic epithelial cells. Molecular biology of the cell 24, 818-831.

Leamon, C.P., Low, P.S., 2001. Folate-mediated targeting: from diagnostics to drug and gene delivery. Drug Discovery Today 6, 44-51.

Li, W.X., Li, Q., Lin, Y., Huang, Y.X., Chen, L., 2016. [Research advances in diagnostic and therapeutic application of long-chain non-coding RNAs in hepatocellular carcinoma]. Zhonghua gan zang bing za zhi = Zhonghua ganzangbing zazhi = Chinese journal of hepatology 24, 628-631.

Luen Tang, B., 2010. Is Rab25 a tumor promoter or suppressor—context dependency on RCP status? Tumor Biology 31, 359-361.

Ma, Y.F., Yang, B., Li, J., Zhang, T., Guo, J.T., Chen, L., Li, M., Chu, J., Liang, C.Y., Liu, Y., 2015. Expression of Ras-related protein 25 predicts chemotherapy resistance and prognosis in advanced non-small cell lung cancer. Genetics and molecular research : GMR 14, 13998-14008.

Merdan, T., Kopec˘ek, J., Kissel, T., 2002. Prospects for cationic polymers in gene and oligonucleotide therapy against cancer. Advanced drug delivery reviews 54, 715-758.

Merlin JL, D.G., Dubessy C, Festor E, Parache RM, Verneuil L, Erbacher P, Behr JP, Guillemin F., 2001. Improvement of nonviral p53 gene transfer in human carcinoma cells using glucosylated polyethylenimine derrivates. Cancer Gene Ther 8, 203-210.

Minai-Tehrani, A., Chang, S.H., Kwon, J.T., Hwang, S.K., Kim, J.E., Shin, J.Y., Yu, K.N., Park, S.J., Jiang, H.L., Kim, J.H., Hong, S.H., Kang, B., Kim, D., Chae, C.H., Lee, K.H., Beck, G.R., Jr., Cho, M.H., 2013. Aerosol delivery of lentivirus-mediated O-

glycosylation mutant osteopontin suppresses lung tumorigenesis in K-ras (LA1) mice. Cellular oncology 36, 15-26.

Nicholson, J.K., Holmes, E., Kinross, J., Burcelin, R., Gibson, G., Jia, W., Pettersson, S., 2012. Host-Gut Microbiota Metabolic Interactions. Science 336, 1262.

Pasut, G., Veronese, F.M., 2009. PEG conjugates in clinical development or use as anticancer agents: an overview. Advanced drug delivery reviews 61, 1177-1188.

Patil, S., Patil, S., Gawali, S., Shende, S., Jadhav, S., Basu, S., 2013. Novel self-assembled lithocholic acid nanoparticles for drug delivery in cancer. RSC Advances 3, 19760-19764.

Paunesku, T., Mittal, S., Protić, M., Oryhon, J., Korolev, S.V., Joachimiak, A., Woloschak, G.E., 2001. Proliferating cell nuclear antigen (PCNA): ringmaster of the genome. International Journal of Radiation Biology 77, 1007-1021.

Pendri A, G.C., Soundararajan S, Bolikal D, Shorr RGL, Greenwald RB 1996. PEG modified anti-cancer drugs: synthesis and biological activity. Journal of Bioactive and comparative polymers 11, 122–134.

Qian, Z.M., Li, H., Sun, H., Ho, K., 2002. Targeted drug delivery via the transferrin receptor-mediated endocytosis pathway. Pharmacological reviews 54, 561-587.
Rao, D.D., Vorhies, J.S., Senzer, N., Nemunaitis, J., 2009. siRNA vs. shRNA: similarities and differences. Advanced drug delivery reviews 61, 746-759.

Roche, J., Nasarre, P., Gemmill, R., Baldys, A., Pontis, J., Korch, C., Guilhot, J., Ait-Si-Ali, S., Drabkin, H., 2013. Global Decrease of Histone H3K27 Acetylation in ZEB1-Induced Epithelial to Mesenchymal Transition in Lung Cancer Cells. Cancers 5, 334-356.

Schuller, H.M., Plummer, H.K., Jull, B.A., 2003. Receptor-mediated effects of nicotine and its nitrosated derivative NNK on pulmonary neuroendocrine cells. The Anatomical Record Part A: Discoveries in Molecular, Cellular, and Evolutionary Biology 270A, 51-58.

Singh, R.P., Deep, G., Chittezhath, M., Kaur, M., Dwyer-Nield, L.D., Malkinson, A.M., Agarwal, R., 2006. Effect of silibinin on the growth and progression of primary lung tumors in mice. Journal of the National Cancer Institute 98, 846-855.

Sokol, R.J., Devereaux, M., Dahl, R., Gumpricht, E., 2006. "Let there be bile"--understanding hepatic injury in cholestasis. J Pediatr Gastroenterol Nutr 43 Suppl 1, S4-9.

Stepanov, I., Upadhyaya, P., Carmella, S.G., Feuer, R., Jensen, J., Hatsukami, D.K., Hecht, S.S., 2008. Extensive metabolic activation of the tobacco-specific carcinogen 4-(methylnitrosamino)-1-(3-pyridyl)-1-butanone in smokers. Cancer epidemiology, biomarkers & prevention : a publication of the American Association for Cancer Research, cosponsored by the American Society of Preventive Oncology 17, 1764-1773.

Subramani, D., Alahari, S.K., 2010. Integrin-mediated function of Rab GTPases in cancer progression. Molecular cancer 9, 312-312.

Sudimack, J., Lee, R.J., 2000. Targeted drug delivery via the folate receptor. Advanced drug delivery reviews 41, 147-162.

Takeuchi, H., Saoo, K., Matsuda, Y., Yokohira, M., Yamakawa, K., Zeng, Y., Miyazaki, M., Fujieda, M., Kamataki, T., Imaida, K., 2006. Dose dependent inhibitory effects of dietary 8-methoxypsoralen on NNK-induced lung tumorigenesis in female A/J mice. Cancer letters 234, 232-238.

Tanos, B., Rodriguez-Boulan, E., 2008. The epithelial polarity program: machineries involved and their hijacking by cancer. Oncogene 27, 6939-6957.

Tehrani, A.M., Hwang, S.K., Kim, T.H., Cho, C.S., Hua, J., Nah, W.S., Kwon, J.T., Kim, J.S., Chang, S.H., Yu, K.N., Park, S.J., Bhandari, D.R., Lee, K.H., An, G.H., Beck, G.R., Jr., Cho, M.H., 2007. Aerosol delivery of Akt controls protein translation in the lungs of dual luciferase reporter mice. Gene therapy 14, 451-458.

Theunissen R, a.R.M., 2008. Particle Image Velocimetry in lung Bifurcation Models. Springer, Berlin, Heidelberg, pp. 73-100.

Thornberry, N.A., Lazebnik, Y., 1998. Caspases: Enemies Within. Science 281, 1312.

Tong, M., Chan, K.W., Bao, J.Y.J., Wong, K.Y., Chen, J.-N., Kwan, P.S., Tang, K.H., Fu, L., Qin, Y.-R., Lok, S., Guan, X.-Y., Ma, S., 2012. Rab25 Is a Tumor Suppressor Gene with Antiangiogenic and Anti-Invasive Activities in Esophageal Squamous Cell Carcinoma. Cancer Res 72, 6024.

Uchenna Agu, R., Ikechukwu Ugwoke, M., Armand, M., Kinget, R., Verbeke, N., 2001. The lung as a route for systemic delivery of therapeutic proteins and peptides. Respiratory research 2, 198-209.

Virág, L., Szabó, C., 2002. The Therapeutic Potential of Poly(ADP-Ribose) Polymerase Inhibitors. Pharmacological reviews 54, 375.

Vllasaliu, D., Fowler, R., Stolnik, S., 2014. PEGylated nanomedicines: recent progress and remaining concerns. Expert Opinion on Drug Delivery 11, 139-154.
Wagner E. Curiel D, C.M., 1994. Delivery of drugs, proteins and genes into cells using transferrin as a ligand for receptor-mediated endocytosis. Advanced drug delivery reviews 14, 113–135.

Wang, S., Konorev, E.A., Kotamraju, S., Joseph, J., Kalivendi, S., Kalyanaraman, B., 2004. Doxorubicin Induces Apoptosis in Normal and Tumor Cells via Distinctly Different Mechanisms: INTERMEDIACY OF H2O2- AND p53-DEPENDENT PATHWAYS. Journal of Biological Chemistry 279, 25535-25543.

Wu, C.H., Wu, G.Y., 1998. Receptor-mediated delivery of foreign genes to hepatocytes. Advanced drug delivery reviews 29, 243-248.

Xu, C.X., Jere, D., Jin, H., Chang, S.H., Chung, Y.S., Shin, J.Y., Kim, J.E., Park, S.J., Lee, Y.H., Chae, C.H., Lee, K.H., Beck, G.R., Jr., Cho, C.S., Cho, M.H., 2008. Poly(ester amine)-mediated, aerosol-delivered Akt1 small interfering RNA suppresses lung tumorigenesis. American journal of respiratory and critical care medicine 178, 60-73.

Yokohira, M., Takeuchi, H., Saoo, K., Matsuda, Y., Yamakawa, K., Hosokawa, K., Kuno, T., Imaida, K., 2008. Establishment of a bioassay model for lung cancer chemoprevention initiated with 4-(methylnitrosamino)-1-(3-pyridyl)-1-butanone (NNK) in female A/J mice. Experimental and toxicologic pathology : official journal of the Gesellschaft fur Toxikologische Pathologie 60, 469-473.

Zhang, J., Wei, J., Lu, J., Tong, Z., Liao, B., Yu, B., Zheng, F., Huang, X., Chen, Z., Fang, Y., Li, B., Chen, W., Xie, D., Luo, J., 2013. Overexpression of Rab25 contributes to metastasis of bladder cancer through induction of epithelial–mesenchymal transition and activation of Akt/GSK-3β/Snail signaling. Carcinogenesis 34, 2401-2408.

Zheng, H.-C., Takano, Y., 2011. NNK-Induced Lung Tumors: A Review of Animal Model. Journal of oncology 2011, 635379.

국문초록

항암치료의 발전에도 불구하고 암은 여전히 전세계 인구의 주요사망원인이다. 항암치료의 어려움 중 하나는 암세포의 전이를 유발하는 비정상적 세포증식이다. 전통적인 항암치료는 급격히 증식하는 암세포가 항암제에 민감하게 반응하는 점을 이용하였으나, 이러한 치료는 증식중인 정상세포에도 비특이적인 독성을 나타낸다. 그러므로 암의 분자적 특성을 이해하는 것과는 별개로, 바이러스를 사용하지 않으면서 약물과 유전자를 전달하는 새로운 항암제를 개발할 필요가 있다. 첫 연구로 잠재적 항암제후보인 리토콜산(LCA) 를 poly(ethyleneglycol) PEG conjugates의 두 가지 형태인 PEG-LCA(PL)과 lactobionic acid (LBA) conjugated PEG-LCA (LPL)로 변형하였다. HepG2 암세포와 LO2 정상세포를 생체외 실험에 사용하였다. 추가적인 검증을 위해서 H-ras 모델마우스에 정맥주사로 C6-loaded PL과 C6-loaded LPL 나노입자를 주입하여 확인하였다.

두 번째 연구에서는 4-(Methylnitrosamino)-1-(3-pyridyl)-1-butanone (NNK)로 폐암을 유발시킨 암컷 A/J마우스모델에서 short hairpin Rab25 RNA (shRab25) 유전자치료효과를 확인하였

다. 이 모델마우스에서는 종양을 유발하기 위하여 NNK를 복강내 주사로 1회 접종하였다. 8주 후 비바이러스성 양이온 전달체로 사용되는 glycerol proxylate triacrylate and spermine (GPT-SPE)를 이용하여 에어로졸 상태로 유전자를 폐에 전달하였다. shRNA 복합체를 이용한 GPT-SPE/Rab25를 담배로 폐암을 유발시킨 A/J 마우스모델에 일주일에 두 번씩 8주 동안 에어로졸 흡입시켰다. 에어로졸 매개 유전자전달방법은 폐조직의 유전자표적화에 사용될 수 있는 비침습적인 대안이다. 반복적인 GPT-SPE/Rab25 shRNA 복합체의 에어로졸 흡입은 폐 종양형성을 크게 억제하였다. 본 연구결과는 간암과 폐암 치료의 새로운 방법과 잠재적 치료성과를 제시하고 있다.

주요어: 항암제, 세포자멸, 간세포특이, 나노입자, 리토콜산, shRab25 에어로졸 전달, 폐암, 유전자치료.

학 번: 2012-30770